ADVANCED FUNCTIONAL MATERIALS
www.afm-journal.de

Oxygen Diffusion in $SrTiO_3$ and Related Perovskite Oxides

*R. A. De Souza**

The transport of oxygen ions plays a central role in determining the performance or the degradation of perovskite-type oxides in applications as diverse as ceramic capacitors, solid electrolytes, memristive devices and all-oxide electronics. In this Feature Article, experimental data reported in the literature for oxygen diffusion in $SrTiO_3$ and in related titanate, zirconate and cerate perovskite oxides [$CaTiO_3$, $BaTiO_3$, $(Na,Bi)TiO_3$, $Pb(Ti,Zr)O_3$, $CaZrO_3$, $SrZrO_3$, $BaZrO_3$, $SrCeO_3$, $BaCeO_3$] are reviewed. The two related aims are to draw attention to discrepancies and to identify reliable diffusion data. The physical limit to the diffusivity of oxygen vacancies in a perovskite oxide is also considered.

1. Introduction

The subject of ion transport in perovskite oxides is both broad and deep, and accordingly one may approach the subject in many different ways. This is due in part to the variety of driving forces that can cause ions to move. Ion motion may occur, for instance, because of a concentration gradient, in which case one speaks of diffusion; or because of an electrical potential gradient, in which case one speaks of drift; or because of a temperature gradient, in which case one speaks of thermodiffusion. In this Feature Article I use diffusion in the solid state as a means of examining oxygen-ion transport in the perovskite-oxide $SrTiO_3$ and related perovskite-oxides.

After introductory sections covering the basics of diffusion, I discuss the experimental determination of, and the differences and the relationships between, the most common diffusion coefficients. The possibilities of diffusion occurring along and across extended defects (dislocations, grain boundaries, surfaces) are also discussed, with the main focus on accelerated diffusion along extended defects and hindered diffusion across extended defects. This first part is rather general, and in writing it, I refer to several books[1–6] and review articles.[7–14] In the second part of the article, the point-defect chemistry of $SrTiO_3$ is first reviewed, after which a critical examination of literature data on oxygen diffusion in $SrTiO_3$, and then in other titanate, zirconate and cerate $A^{II}B^{IV}O_3$ perovskite-oxides, is given. For details on oxygen diffusion in $A^{III}B^{III}O_3$ perovskite-oxides, the interested reader is referred to reviews in the literature.[15–17]

R. A. De Souza
Institute of Physical Chemistry
RWTH Aachen University and JARA-FIT
52056 Aachen, Germany
E-mail: desouza@pc.rwth-aachen.de

DOI: 10.1002/adfm.201500827

2. Definitions

There are two complementary approaches to treating diffusion: the macroscopic approach based on Fick's empirical equations; and the microscopic approach based on atomic mechanisms and on random-walk theory. The macroscopic definition provides the experimental basis for determining diffusion coefficients. At no point in the macroscopic treatment, however, does the atomic nature of matter enter into the treatment. Nonetheless, diffusion in solids results from many individual jumps of the diffusing particles, and it is mediated by point defects, such as vacancies and interstitials. The benefit of the microscopic approach, then, is that it provides the theoretical basis for interpreting and expressing diffusion coefficients in terms of atomic quantities, such as point-defect concentrations, atomic jump distances and activation barriers.

2.1. Macroscopic Approach

The flux of component i passing through unit area of a reference plane per unit time, j_i, is given by Fick's first law, written in one dimension as

$$j_i = -D_i \frac{\partial c_i}{\partial x} \tag{1}$$

The factor of proportionality between the flux and the negative concentration gradient is D_i, the diffusion coefficient of i in the specific system.

In most cases, the amount of the diffusing component is conserved during the process of diffusion. This statement is expressed by the continuity equation, which for diffusion in one dimension is

$$-\frac{\partial j_i}{\partial x} = \frac{\partial c_i}{\partial t} \tag{2}$$

Substitution of Equation (1) into Equation (2) yields Fick's Second Law,

$$\frac{\partial c_i}{\partial t} = \frac{\partial}{\partial x}\left(D_i \frac{\partial c_i}{\partial x} \right) \tag{3}$$

which, if the diffusion coefficient is independent of position, reduces to

$$\frac{\partial c_i}{\partial t} = D_i \frac{\partial^2 c_i}{\partial x^2} \tag{4}$$

The second-order partial differential equation, Equation (3) or (4), is sometimes called the diffusion equation. Although the one-dimensional treatment is often sufficient, Fick's first law is easily generalised to the three-dimensional case:

$$\mathbf{j}_i = -\mathbf{D}_i \nabla c_i \tag{5}$$

in which $\mathbf{j}_i$ is the vector flux; the Nabla operator ∇ acts on the scalar concentration field $c_i(x, y, z)$; and $\mathbf{D}_i$ is a symmetric second-rank tensor (in cubic crystals, it reduces to the single scalar quantity D_i).[2] It is important to note that, although Equation (1) gives the macroscopic definition of a diffusion coefficient, the true driving force for diffusion is not the gradient in the concentration of i (∇c_i), but the gradient in its chemical potential ($\nabla \mu_i$); see also Section 3. At chemical equilibrium, the gradient in the chemical potential of all mobile components is zero.

2.1.1. Dependence of the Diffusion Coefficient on Characteristic Thermodynamic Parameters

Phenomenologically one often observes that, as a function of temperature T, the diffusion coefficient obeys Arrhenius-type behavior,

$$D_i(T) = D_i^{\circ} \exp\left(-\frac{\Delta H_{D_i}}{k_B T}\right) \tag{6}$$

that is, the behavior is characterized by just two quantities, the pre-exponential factor D_i° and the activation enthalpy of diffusion ΔH_{D_i}. Values of ΔH_{D_i} determined experimentally for oxides[18–20] may be as low as some tenths of an eV or as high as 10 eV, but are generally of the order of 10^0 eV.

For a binary metal oxide MO, the Gibbs phase rule stipulates that three variables are required to define the system thermodynamically. Two variables are temperature and hydrostatic pressure; the third variable is commonly chosen to be the oxygen activity $a\mathrm{O}_2$ (as experimentally it is easier to define and to vary $a\mathrm{O}_2$ than $a\mathrm{M}$, the activity of the metallic component; furthermore $a\mathrm{O}_2$ can be varied experimentally over tens of orders of magnitude). Values of the diffusion coefficient measured as a function of $a\mathrm{O}_2$ at constant temperature are found to obey a power law, with the power-law exponents $m_{a\mathrm{O}_2}$,

$$m_{a\mathrm{O}_2} = \left(\frac{\partial \ln D_i}{\partial \ln a\mathrm{O}_2}\right)_T \tag{7}$$

Considered over a suitably large range of oxygen partial pressures, $m_{a\mathrm{O}_2}$ may take characteristic values of $\pm\frac{1}{6}, \pm\frac{1}{4}, \pm\frac{1}{2}$, etc., see Section 5.4.

In order to interpret and understand the activation energy of diffusion or the power-law exponent, one must consider diffusion from a microscopic standpoint.

2.2. Microscopic Definition

The microscopic definition of the diffusion coefficient D_i comes, independently, from Einstein and from Smoluchowski.

Roger A. De Souza obtained a B. Eng. in Material Science and Engineering in 1992 and a Ph.D. in Materials Science in 1996 from Imperial College London. After spending two years as a post-doctoral researcher at the University of Karlsruhe, he moved to the Max-Planck Institute for Solid State Research in Stuttgart. In 2002 he joined the Institute of Physical Chemistry at RWTH Aachen University, where he received his professorial degree (Habilitation). His research, encompassing both experimental and computational approaches, focuses on complex oxides for energy and information technologies, and in particular, on characterizing and understanding transport processes in these oxides and at their extended defects.

They related the mean square displacement $\langle x^2 \rangle$ of the diffusing species in the x-direction to the x-component of the diffusion coefficient, D_i^x, and to the time interval t during which diffusion takes place:[1,2,5]

$$\left\langle x_i^2 \right\rangle = 2D_i^x t \tag{8}$$

This is now known as the Einstein relation or as the Einstein–Smoluchowski relation. For diffusion in an isotropic, three-dimensional medium, $\left\langle x_i^2 \right\rangle = \left\langle y_i^2 \right\rangle = \left\langle z_i^2 \right\rangle = \left\langle R_i^2 \right\rangle / 3$, the mean square displacement is given by

$$\left\langle R_i^2 \right\rangle = 6D_i t \tag{9}$$

From the theory of random walks, one obtains for an uncorrelated random walker that executes a series of n consecutive jumps, each of distance a, from one site to a neighboring site (a in oxides is thus of the order of a few Å),

$$\left\langle R_i^2 \right\rangle = na^2 \tag{10}$$

Combining Eqs. (9) and (10), and introducing the jump rate of the particle to one of its Z neighbors, $\Gamma_i Z = n/t$, one obtains

$$D_i = \frac{1}{6} a^2 Z \Gamma_i \tag{11}$$

2.2.1. Diffusion Coefficients of Defects and Ions

In general there will be a considerable difference between the diffusion coefficient of the defect, D_{def}, and the diffusion coefficient of the ion, D_{ion}. To see why this is so, we consider the concrete example of oxygen ions migrating in an oxide by a vacancy mechanism. The diffusion coefficient of the vacancies is (see Equation (11))

$$D_V = \frac{1}{6}a^2 Z\Gamma_V \tag{12}$$

whereas the diffusion coefficient of the oxygen ions is

$$D_O = \frac{1}{6}a^2 Z\Gamma_O \tag{13}$$

Each time a vacancy moves, an ion has to move, as the two species swap places. Thus, the total number of displacements of the ions and of the vacancies has to be equal

$$\Gamma_O[O] = \Gamma_V[V] \tag{14}$$

with $[i]$ denoting the concentration of i. For a dilute solution of vacancies, the site fraction of vacancies, n_V, is by definition many orders of magnitude less than unity, and it can thus be approximated by $n_V \approx [V]/[O]$. Hence, by combining Equations (12)–(14), we obtain

$$D_O = D_V \frac{[V]}{[O]} \approx D_V n_V \tag{15}$$

Thus, D_O and D_V will differ by the factor $n_V \ll 1$. One should note that n_V may vary considerably with temperature, oxygen activity and dopant concentration (see Section 5). D_V, at least for dilute solutions of vacancies, is independent of n_V, and as we will see later, only dependent on temperature. One consequence of Equation (15) is that the mean square displacement of a vacancy, $\langle R_V^2 \rangle$, will be orders of magnitude larger than the mean square displacement of an oxygen ion, $\langle R_O^2 \rangle$.

2.2.2. Activation Barriers

In a simple approximation of the ion-hopping process—a complicated many-body problem[21]—one can relate the jump rate Γ to the height of the activation barrier ΔG_{mig} through an Arrhenius law,

$$\Gamma = \nu_0 \exp\left(\frac{-\Delta G_{mig}}{k_B T}\right) \tag{16}$$

where the prefactor ν_0 denotes an attempt frequency of the order of the Debye frequency of the compound, k_B is Boltzmann's constant, and T is the absolute temperature. ΔG_{mig} is the Gibbs activation energy of migration, and it corresponds to the difference in the system's Gibbs energy between the initial and saddle-point configurations. It can be expressed in terms of an activation enthalpy of migration, ΔH_{mig}, and an activation entropy of migration, ΔS_{mig},

$$\Delta G_{mig} = \Delta H_{mig} - T\Delta S_{mig} \tag{17}$$

Combining Equations (15)–(17), we thus find, for the case of oxygen-ion diffusion in a cubic system with a dilute solution of oxygen vacancies, that the self-diffusion coefficient of oxygen is given by

$$D_O(T, aO_2) = n_V(T, aO_2) D_V(T) = n_V(T, aO_2)\frac{1}{6}a^2 Z\nu_0 \exp\left(\frac{\Delta S_{mig,V}}{k_B}\right)\exp\left(\frac{-\Delta H_{mig,V}}{k_B T}\right). \tag{18}$$

3. Types of Diffusion Experiments

There are a bewildering variety of ways in which to carry out diffusion experiments, and thus, a bewildering variety of diffusion coefficients that one can obtain. For oxide materials, the three most commonly determined coefficients are D^*, the tracer diffusion coefficient; D^δ, the chemical diffusion coefficient; and D^σ, the conductivity diffusion coefficient.[6] In the following we will examine, first, what the basics of the three diffusion experiments are, and second, how the respective diffusion coefficients are related to the self-diffusion coefficients of the ions D_{ion}, or of the defects D_{def}. We consider, again, a generic metal oxide MO, in order to emphasise that the methods are applicable to all oxides, not just perovskites.

In order to obtain expressions relating the diffusion coefficients to one another, we require a theoretical framework to treat these processes, and the most convenient theoretical framework for treating these and other transport processes is linear irreversible thermodynamics.[22] For example, for a system that contains the mobile charge carriers i and k (which may be ionic or electronic species) and that is exposed to a temperature gradient, one can express, according to linear irreversible thermodynamics, the vector fluxes of the two charge carriers and the vector flux of heat as

$$\begin{aligned} \mathbf{j}_i &= L_{ii}\mathbf{X}_i + L_{ik}\mathbf{X}_k + L_{iQ}\mathbf{X}_Q \\ \mathbf{j}_k &= L_{ki}\mathbf{X}_i + L_{kk}\mathbf{X}_k + L_{kQ}\mathbf{X}_Q \\ \mathbf{j}_Q &= L_{Qi}\mathbf{X}_i + L_{Qk}\mathbf{X}_k + L_{QQ}\mathbf{X}_Q \end{aligned} \tag{19}$$

that is, in terms of phenomenological transport coefficients L and general thermodynamic driving forces, $\mathbf{X}$. Equation (19) states that a flux of i, say, can result directly from the driving force $\mathbf{X}_i$, but also indirectly from the driving forces $\mathbf{X}_k$ and $\mathbf{X}_Q$. The thermodynamic driving force for heat transport is given by $\mathbf{X}_Q = -(1/T)\nabla T$; for the charge carrier i, the thermodynamic driving force is given, in the absence of external forces, by $\mathbf{X}_i = -T\nabla(\eta_i/T)$, where η_i denotes the electrochemical potential of i and is defined as (z_i is the charge number of i)

$$\eta_i = \mu_i + z_i e\phi \tag{20}$$

The off-diagonal elements of the matrix of L coefficients lead to "cross" effects, such as thermoelectricity (L_{eQ}) and thermodiffusion (L_{iQ}) and are thus also known as cross-coefficients. Onsager's reciprocity theorem states that, in the absence of a magnetic field, the matrix of L coefficients is symmetric, that is, $L_{ik} = L_{ki}$, and so forth. It is noted that an oxide was used as a model system to verify Onsager's theorem experimentally.[23]

Let us now for simplicity restrict the treatment to the one dimensional case and to ideal solutions. Transforming Equation (19) to the "reduced" heat formulation;[7,13,14,24] assuming $L_{iQ} = L_{Qi}$; and using $L_{ii} = D_i[i]/k_B T$; one can write the flux of i as

$$j_i = -\frac{D_i[i]}{k_B T}\left[\frac{\partial \eta_i}{\partial x} + \left(\overline{S}_i + \frac{Q_i}{T}\right)\frac{\partial T}{\partial x}\right] \quad (21)$$

where $\overline{S}_i$ is the partial molar entropy and Q_i the reduced heat of transport of charge carrier i. Thus, we perceive that, in general, a flux of i can be driven by a gradient in chemical potential (diffusion), by a gradient in electrical potential (drift) and by a gradient in temperature (thermodiffusion). The term $(\overline{S}_i + Q_i/T)$ may be positive or negative, and thus depending on its sign, i may move down or up the temperature gradient.

In the isothermal case, to which the three diffusion experiments refer, Equation (21) reduces to

$$j_i = -\frac{D_i[i]}{k_B T}\left[\frac{\partial \mu_i}{\partial x} + z_i e\frac{\partial \phi}{\partial x}\right] \quad (22)$$

The procedures for deriving the various diffusion coefficients from Equation (19) or from from Equation (22) are given in detail elsewhere;[7,8,11] for reasons of limited space, only the end results are reproduced in the relevant sections below. Furthermore, only the simplest cases are considered: many complications are possible.[6,11,14,25]

3.1. Chemical Diffusion

Consider an oxide of composition $MO_{1-\delta}$ in chemical equilibrium with the surrounding gas phase, that is, the chemical potential of oxygen is constant throughout the oxide and equal to that in the gas phase. A difference in the chemical potential of oxygen between the sample and the surrounding gas phase is now effected (either by changing the system's temperature or the oxygen activity of the gas phase), with the result that oxygen is either incorporated or removed from the oxide (see **Figure 1**). The nonstoichiometry changes, therefore, from its original value δ to a final value $\delta+\Delta\delta$. The process whereby this takes place ($MO_{1-\delta}+\Delta\delta\cdot\frac{1}{2}O_2 \rightarrow MO_{1-\delta+\Delta\delta}$) is called chemical diffusion. The chemical diffusion coefficient, according to Fick's first law (Equation (1)), is denoted by D_i^δ, D_i or $D_{i,\mathrm{chem}}$: the true driving force, however, is the gradient in the chemical potential of oxygen.[11]

Although formally oxygen is incorporated into the oxide as a neutral component ("O"), at the microscopic scale there is coupled transport of charged species, otherwise known as ambipolar diffusion. Let us assume that our oxide $MO_1.\delta$ has oxygen vacancies, $V_O^{\cdot\cdot}$, and electrons, e', as the dominant mobile defects. As oxygen is incorporated, there will be a flux of vacancies $j_{V_O^{\cdot\cdot}}$ and a flux of electrons $j_{e'}$ towards the surface, these two fluxes being given by (see Equation (22))

$$\begin{aligned} j_{V_O^{\cdot\cdot}} &= -\frac{D_{V_O^{\cdot\cdot}}[V_O^{\cdot\cdot}]}{k_B T}\left[\frac{\partial \mu_{V_O^{\cdot\cdot}}}{\partial x} + 2e\frac{\partial \phi}{\partial x}\right] \\ j_{e'} &= -\frac{D_{e'}[e']}{k_B T}\left[\frac{\partial \mu_{e'}}{\partial x} - e\frac{\partial \phi}{\partial x}\right] \end{aligned} \quad (23)$$

These two fluxes are not independent, however, since $2j_{V_O^{\cdot\cdot}} - j_{e'} = 0$. Furthermore, the internal gradient in the electrical potential, $-\partial\phi/\partial x$ (also known as the Nernst field), is common to both fluxes; this coupling has the effect of accelerating the slower moving moiety and slowing down the faster moving one. The detailed analysis yields

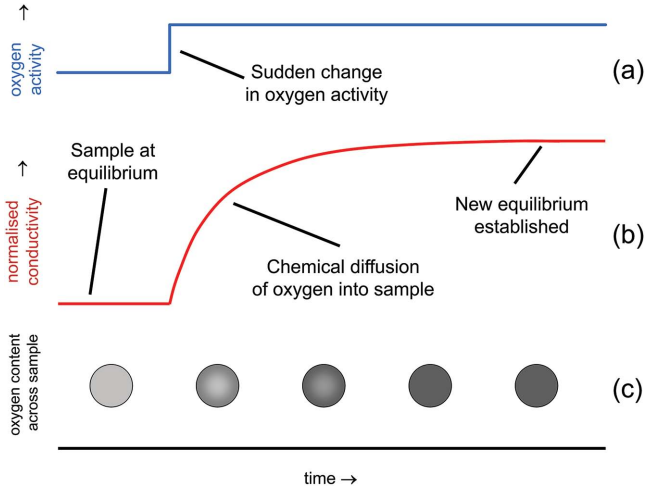

Figure 1. The chemical diffusion experiment consists, for example, of a) raising instantaneously the oxygen activity in the gas phase, and b) then monitoring as a function of time the change in a characteristic sample property, that is, c) one that depends on the oxygen content of the sample, such as the electrical conductivity, as the sample attains the new equilibrium with the gas phase.

$$D_O^\delta = \frac{D_{V_O^{\cdot\cdot}}[V_O^{\cdot\cdot}]\quad D_{e'}[e']}{4D_{V_O^{\cdot\cdot}}[V_O^{\cdot\cdot}] + D_{e'}[e']}\left(\frac{1}{2}\frac{\partial \ln aO_2}{\partial c_O}\right) \quad (24)$$

It is clear from Equation (24) that the chemical diffusion coefficient of oxygen in $MO_{1-\delta}$, D_O^δ, may exhibit rather complex behavior as a function of temperature and oxygen activity, depending on how the individual parameters vary with T and aO_2.

In some cases, Equation (24) reduces to a simpler form: If, for instance, the two defects are dilute, non-interacting species, we find

$$D_O^\delta = \frac{D_{V_O^{\cdot\cdot}}[V_O^{\cdot\cdot}]\quad D_{e'}[e']}{4D_{V_O^{\cdot\cdot}}[V_O^{\cdot\cdot}] + D_{e'}[e']}\left(\frac{1}{[V_O^{\cdot\cdot}]} + \frac{4}{[e']}\right) \quad (25)$$

Furthermore, if the electrons are more mobile than the vacancies, $D_{e'} \gg D_{V_O^{\cdot\cdot}}$, and if electroneutrality is given by $[e'] = 2[V_O^{\cdot\cdot}]$, we obtain

$$D_O^\delta = 3D_{V_O^{\cdot\cdot}} \quad (26)$$

(More complicated situations may also give this simple expression).[6,26,27] Equation (26) tells us that D_O^δ is given by the diffusivity of the slowest moving defect (in this case: vacancies) multiplied by an "acceleration factor" (=3) because of the coupling through the Nernst field with the faster moving electrons. In this special case, the activation enthalpy of chemical diffusion is the activation enthalpy of vacancy migration: $\Delta H_{D_O^\delta} = \Delta H_{\mathrm{mig},V_O^{\cdot\cdot}}$.

With knowledge of D_O^δ, one can predict the time τ necessary for the change in a sample's nonstoichiometry to proceed, say, to 99% completion. A useful order-of-magnitude approximation for a slab sample of thickness $2l$ is $\tau_{D^\delta} \sim l^2 / 2D_O^\delta$. In certain cases, for instance for thin samples, the kinetics of the stoichiometry change are governed by the surface reaction (see Section 4), and the time required is $\tau_{k^\delta} \sim 5l / 2k_O^\delta$. For the intermediate regime, where both bulk diffusion and surface kinetics are important, $\tau_{D^\delta} \sim \tau_{k^\delta}$, a good approximation is $\tau \approx \tau_{D^\delta} + \tau_{k^\delta}$.

3.2. Tracer Diffusion

A tracer diffusion experiment refers to the use of radioactive or stable isotopes—chemically identical, labelled species i^*—to examine self-diffusion in condensed matter. Since one can distinguish between i^* and i, the motion of the indistinguishable i particles can be followed with the help of the tracers, i^*.[11] Tracer diffusion experiments are performed at constant sample composition. For our example oxide $MO_{1-\delta}$, this corresponds in the case of the cation tracer to $MO_{1-\delta} \rightarrow (M_{1-\alpha}M^*_\alpha)O_{1-\delta}$ and in the case of the anion tracer (see **Figure 2**) to $MO_{1-\delta} \rightarrow M(O_{1-\alpha}O^*_\alpha)_{1-\delta}$. The only driving force is the gradient in the chemical potential of the tracer (and is thus purely entropic); the chemical potentials of M and O are constant throughout the system.

The measured tracer diffusion coefficient of species i is related to the self-diffusion coefficient through the tracer correlation factor f^*,

$$D_i^* = f^* D_i \tag{27}$$

f^* varies according to the migration mechanism (interstitial, vacancy, colinear/non-colinear interstitialcy) and the geometry of the sublattice on which diffusion takes place.[2,5] f^* reflects the fact that tracer species do not necessarily perform an uncorrelated random walk. Let us consider the case of vacancy migration on a simple cubic sublattice. The vacancies may move in all six migration directions with equal probability. This is not true, however, for the tracer species: If a vacancy and a tracer have just exchanged places, the most likely jump of the tracer is back to its original position. Its mean square displacement $\langle (R_{i^*})^2 \rangle$ is hence less than that of a random walker, $\langle R_i^2 \rangle$; f^* is the ratio of the two, $f^* = \langle (R_{i^*})^2 \rangle / \langle R_i^2 \rangle$, and thus takes values between zero and unity. The detailed analysis with linear irreversible thermodynamics starts from Equation (19); considers three fluxes, for example, for a vacancy mechanism j_i, j_{i^*} and j_V; and yields f^* in terms of L_{ii} and L_{ii^*}.[7,8] f^* deviates from unity if L_{ii^*} deviates from zero. For a dilute solution of oxygen vacancies in a cubic perovskite, $f^* = 0.69$.[28]

The activation enthalpy of tracer diffusion, $\Delta H_{D_i^*}$ is easily determined by performing measurements as a function of temperature (at constant oxygen activity), but it is not so easy to interpret. For the case of vacancy transport, we find upon combining Equations (15) and (27),

$$D_i^* = f^* D_{V_O^{\cdot\cdot}} n_{V_O^{\cdot\cdot}} \tag{28}$$

Since the dependence on temperature of $D_{V_O^{\cdot\cdot}}$ and $n_{V_O^{\cdot\cdot}}$ can be expressed in exponential functions,

$$D_i^* = f^* D^\circ_{V_O^{\cdot\cdot}} \exp\left(-\frac{\Delta H_{\mathrm{mig},V_O^{\cdot\cdot}}}{k_B T}\right) n^\circ_{V_O^{\cdot\cdot}} \exp\left(-\frac{\Delta H_{\mathrm{gen},V_O^{\cdot\cdot}}}{k_B T}\right) \tag{29}$$

with $\Delta H_{\mathrm{mig},V_O^{\cdot\cdot}}$ being the activation enthalpy of vacancy migration and $\Delta H_{\mathrm{gen},V_O^{\cdot\cdot}}$, reflecting the change in vacancy concentration with temperature, we find

$$\Delta H_{D_i^*} = \Delta H_{\mathrm{mig},V_O^{\cdot\cdot}} + \Delta H_{\mathrm{gen},V_O^{\cdot\cdot}} \tag{30}$$

Consequently, interpretation of the measured activation enthalpy of tracer diffusion requires quantitative knowledge of the defect chemistry (how exactly does the relevant defect concentration vary with temperature?). $\Delta H_{\mathrm{gen},V_O^{\cdot\cdot}}$, it should be noted, can be zero ($[V_O^{\cdot\cdot}]$ independent of temperature), or positive ($[V_O^{\cdot\cdot}]$ increasing with increasing temperature), in which case it can take values up to several eV. Hence, depending on the particular case, it may be much larger than, much smaller than, or even comparable to $\Delta H_{\mathrm{mig},V_O^{\cdot\cdot}}$.

3.3. Conductivity

In a sense, determining the electrical conductivity of a sample is the simplest of the three transport experiments. One applies an electrical potential gradient $\nabla\phi$ to a sample and measures the resulting electrical current density I. The electrical conductivity σ is obtained from Ohm's law

$$I = -\sigma \nabla \phi \tag{31}$$

There are, however, several possible complications to this simple experiment. First, and most important, is that all mobile charged species contribute to the measured conductivity, all ionic and all electronic charge carriers, each conductivity contribution being the product of the concentration $[i]$, charge $z_i e$ and mobility u_i

$$\sigma_{\mathrm{tot}} = \sum_i \sigma_i = \sum_i [i] z_i e u_i \tag{32}$$

Generally, the mobilities of electronic charge carriers are orders of magnitude larger than

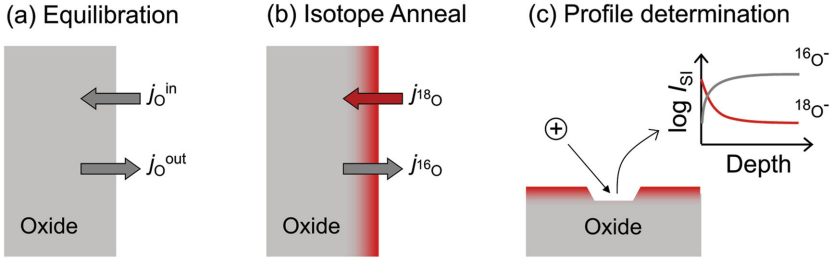

Figure 2. The tracer diffusion experiment:[12] a) Equilibration of the oxide sample in oxygen of normal isotopic abundance at given T and aO_2. b) Isotope anneal at the same T and $aO2$, in an ^{18}O-enriched gas for a given time. c) The isotope profile in the oxide is determined by an ion-beam-analysis method, such as Secondary Ion Mass Spectrometry (SIMS).

those of ionic charge carriers; hence a small concentration of electrons or holes (minority defects) may provide the dominant contribution to the electrical conductivity. To isolate the ionic contribution, one may have to use the appropriate electron-blocking but ion-conducting electrodes, or else determine, in addition to the total conductivity, the ionic transference number t_{ion}, that is, the proportion of the conductivity carried by the ions, $t_{ion} = \sigma_{ion}/\sigma_{tot}$ (through emf measurements on a Nernst cell). The second complication is that the conductivity of Equation (31) depends, in principle, on the applied electrical potential gradient: It is only for small driving forces, specifically for $|az_ie\nabla\phi| \ll 2k_BT$, that the conductivity is independent of driving force, that is, Equation (31) constitutes a linear law. (NB: At $T = 300$ K, a field of ≈ 2 MV cm^{-1} is required to increase the oxygen-ion conductivity by a factor of 2.) Third, the sample's electrical response may be dominated by that of the electrodes, for instance, and obtaining the bulk contribution requires either the use of 4-point measurement geometries in dc mode or frequency-dependent impedance spectroscopy studies.

Having determined the ionic conductivity of the bulk phase in the linear regime, one can now calculate the conductivity diffusion coefficient with the aid of the Nernst–Einstein equation,

$$D_i^{\sigma} = \sigma_i \frac{k_B T}{[i](z_i e)^2} \tag{33}$$

There are various routes to derive Equation (33), but all of them, it is emphasised, assume the charge carriers under consideration to be non-interacting and dilute.[3,9] From linear irreversible thermodynamics, for example, one considers a sample of uniform composition ($\nabla\mu_i = 0$) and temperature ($\nabla T = 0$), to which a gradient in the electrical potential $\nabla\phi$ (as the sole thermodynamic driving force) is applied. Comparison of Equation (22), which is only valid for dilute, non-interacting charge carriers, with Equation (31) yields Equation (33). It is to be noted that, although in general $D_{ion} \neq D_{def}$ and one can measure both independently, there is only one measured conductivity, $\sigma_{ion} \equiv \sigma_{def}$. Thus, from a measured conductivity, one can calculate D_{ion} if one knows [ion], and D_{def} if one knows [def].

4. Mass Transport Along and Across Extended Defects

Real oxide samples, one should recognise, are not single crystals containing only point defects: extended defects, such as dislocations and grain boundaries, will in general also be present. In addition, real samples are finite in extent, and thus are bounded by surfaces or interfaces with other phases. A variety of paths may therefore be available for diffusing species (see **Figure 3**); one differentiates between:[2,4,10] 1) bulk diffusion (also termed volume or lattice diffusion), which refers to mass transport within a single grain; 2) grain-boundary diffusion, which refers to mass transport along the region of crystallographic misorientation between two grains; 3) dislocation or 'pipe' diffusion, which refers to mass transport along dislocations; and 4) surface diffusion, which refers to mass transport along a crystal surface.

For a given material, the diffusion coefficient of component i along a grain boundary, dislocation or surface (D_i^{gb}, D_i^{dis}, D_i^{s} respectively) will vary according to the structural characteristics of the extended defect. In the case of planar defects (grain boundaries and surfaces), the diffusion coefficient will be a function of the interface (mis)orientation; D_i^{gb}, for example, will vary with the parameters that characterise the grain boundary: the tilt and twist axes, the tilt and twist angles, and the interface plane. Measurements on polycrystals will thus provide an average over all the grain boundaries contained within the investigated volume. In the case of line defects, D_i^{dis} will vary according to the dislocations' character (edge/screw) and its Burgers vector. These alternative paths offered by extended defects become important, if diffusion in the bulk is slow. In such cases, this fast-path diffusion, or short-circuit diffusion, may contribute significantly to mass transport or may even govern the overall behavior.

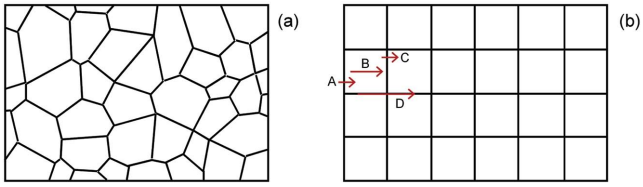

Figure 3. Mass transport processes in a polycrystal. a) Cross-section through a polycrystalline solid. b) The brick-layer model, an idealised representation of the microstructure shown in a). The arrows indicate possible transport processes, with the length of an arrow being inversely proportional to the resistance of the associated process. A: hindered transport across a surface; B: transport in the grain bulk; C: hindered transport across a grain boundary; D: enhanced transport along a grain boundary.

Why should diffusion along these extended defects occur faster than in the bulk? The atomic arrangements within grain boundaries and within dislocation cores are considered to be more open than in the bulk phase, suggesting less hindrance for the migrating species and thus accelerated rates of mass transport. Although there is much experimental data that confirms this picture for metallic systems,[29–31] it is far from certain that this picture is also universally applicable to oxides.[32] In an ionic solid, an ion diffusing along an extended defect may have to pass, in a migration jump, ions of the same polarity—a process that is avoided in the bulk phase. Furthermore, the intrinsic structure of the extended defects may offer preferential sites for point defects: as a result there may be a high concentration of defects within the extended defects, but they are locked into the structure and thus essentially immobile.[33] A more open arrangement within the extended defect does not, therefore, guarantee accelerated rates of ion transport. In addition, the extended defects may be electrostatically charged, with global charge neutrality being satisfied by attendant, enveloping tubes of space charge in which the concentrations of mobile, charged point-defects are modified drastically from their values in the electroneutral bulk.

In addition to fast-path diffusion processes that take place in parallel to diffusion in the bulk phase, there may be slower processes in series with bulk diffusion (see Figure 3). Hindered mass transport across interfaces (surfaces, grain boundaries) constitute such slower serial processes, and they may also influence (or even govern) the overall diffusion behavior. Here, one describes the flux across the interface in terms of a transfer

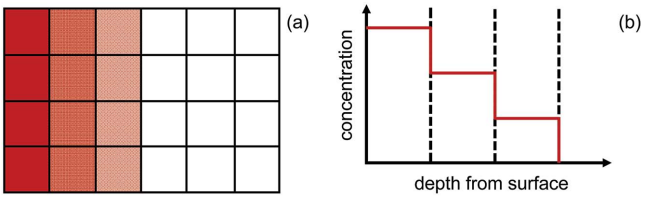

Figure 4. Diffusion in a polycrystalline sample with grain size w in which transport across grain boundaries is slow ($k_i^{gb} \ll D_i / w$) and diffusion along grain boundaries is negligible. a) Cross-section of a polycrystal: diffusant enters the sample from the left. b) Concentration profiles across the polycrystal, showing the drops in concentration (Δc_i) at the grain boundaries (whose positions are indicated by the dashed, vertical lines).

coefficient k_i and the drop in concentration across the interface, Δc_i, in the direction of the flux:

$$j_i = k_i \Delta c_i \tag{34}$$

The case of transport being limited by grain boundaries is illustrated schematically in **Figure 4**.

Why may transport across an interface be hindered? What does k_i refer to, on a microscopic level? There are several possible causes for k_i taking a finite value. At a grain boundary, for example, the crystallographic mismatch between the two grains may conceivably result in the matter flux being diminished, either because of the considerable perturbations of the bulk structure at the interface itself or because of differences in the orientations of the grains in layered structures. The magnitude of such effects are probably small, though. In contrast, huge effects are observed, where space-charge layers, depleted of mobile charge carriers, are present at the grain boundaries.[6] Huge effects are also observed in polycrystalline samples, in which a second phase covers each grain; in oxygen-ion conductors, for example, such second phases are often SiO_2-based compounds that exhibit much lower rates of oxygen transport.[34]

In the case of oxygen transport across a surface, that is, across a gas|solid interface, the transfer coefficient k_O^s characterises the exchange flux of the dynamic equilibrium between oxygen in the gas phase and oxygen in the solid. The forward reaction, for example, requires, in addition to several charge transfer steps, the adsorption and the dissociation of oxygen molecules on the surface, and the incorporation of the resulting oxygen moiety into the crystal lattice. The most likely rate determining step is either dissociation or charge transfer leading to dissociation.[35]

5. Defect Chemistry of Titanate Perovskites

The behavior of point defects in $SrTiO_3$ is understood to a remarkable degree. This is due to the considerable effort, both experimental and theoretical, that has been, and that continues to be, devoted to this subject.[36–59] The other perovskite oxides have received far less attention, but the available literature (e.g., for $BaTiO_3$,[60–63] for $CaTiO_3$)[64–66] indicates that the defect behavior, in most cases, is qualitatively the same. That is to say, the defect equilibria are the same as for $SrTiO_3$, but the equilibrium constants differ, of course, depending on the particular composition.

Given the close-packed nature of the ABO_3 perovskite structure, the dominant ionic point defects are far more likely to be vacancies than interstitials. Indeed, theoretical calculations confirm that Schottky disorder reactions exhibit much lower enthalpies than Frenkel and anti-Frenkel reactions.[52,53] In $SrTiO_3$, the dominant disorder is found both experimentally[47] and theoretically[52,53] to be SrO partial Schottky (in $BaTiO_3$, though, it is TiO_2 partial Schottky disorder).[61,63] Under most conditions, however, defect concentrations in ABO_3 perovskites are dictated not by an intrinsic, Schottky-disorder reaction but by purposely added dopants (or by inadvertently included impurities). [Nominally undoped Pb(Zr,Ti)O_3 and (Na,Bi)TiO_3 represent exceptions owing to the facile loss of Pb and Bi, respectively, at high temperatures; see later.] In this article, the focus is on $SrTiO_3$ that purposely contains acceptor-dopant cations and on nominally undoped $SrTiO_3$, which is typically also acceptor-doped, as it contains impurities such as Al, Fe and Mg that substitute for Ti.[37,58]

The aim of defect-chemical modelling is to predict the concentrations of point defects, [def], as a function of the thermodynamic variables, such as temperature T and oxygen activity aO_2. To this end, one specifies the relevant defect equilibria, and with knowledge of the associated equilibrium constants, one can solve the system of linear equations to obtain [def]. There are various defect equilibria that may be active in $SrTiO_3$, the number increasing with increasing temperature. Essentially, one can differentiate between low-, intermediate- and high-temperature regimes. The transition temperatures between the three regimes are not well defined, but depend on the sample geometry and the amount of time given to the system to reach equilibrium (see Section 5.4). We will now consider the three regimes in order of increasing temperature.

5.1. Low-Temperature Regime

In the first regime, that is, at temperatures below $T \approx 550$ K, only internal equilibria are active: the sample is not in equilibrium with the surrounding atmosphere. The most important reaction is the generation of electrons and holes by thermal excitation across the band gap,

$$\text{null} \rightleftharpoons \text{h}^{\cdot} + \text{e}' \tag{35}$$

with equilibrium constant

$$[\text{e}'][\text{h}^{\cdot}] = K_{\text{eh}}(T) = N_{\text{VB}}(T) N_{\text{CB}}(T) \exp\left(\frac{-E_{\text{bg}}(T)}{k_{\text{B}}T}\right) \tag{36}$$

where $N_{\text{VB}}(T)$ and $N_{\text{CB}}(T)$ are the temperature-dependent density of states at the valence band (VB) and conduction band (CB) edges, and $E_{\text{bg}}(T)$ is the temperature-dependent thermal bandgap; $E_{\text{bg}}(T = 0\ \text{K}) = 3.2$ eV.[38,41,47] If, instead of Equation (36), the approximate form with a temperature-independent pre-exponential factor is used,

$$[\text{e}'][\text{h}^{\cdot}] = K_{\text{eh}}(T) = K^{\circ}_{\text{eh}} \exp\left(\frac{-E^{*}_{\text{bg}}}{k_{\text{B}}T}\right) \tag{37}$$

E_{bg}^{*} is higher than 3.2 eV, as it incorporates the T^3-dependence of $N_{VB}(T)N_{CB}(T)$.[59]

The other internal, electronic reactions of importance are the ionization reactions of ionic defects. The ionization of oxygen vacancies, for instance, yields free electrons according to

$$V_O^{\times} \rightleftharpoons V_O^{\bullet} + e' \tag{38}$$

$$V_O^{\bullet} \rightleftharpoons V_O^{\bullet\bullet} + e' \tag{39}$$

with

$$\frac{[V_O^{\bullet}][e']}{[V_O^{\times}]} = K_{V_O^{0/1}}(T) = K^{\circ}_{V_O^{0/1}} \exp\left(\frac{-\Delta H_{V_O^{0/1}}}{k_B T}\right), \tag{40}$$

$$\frac{[V_O^{\bullet\bullet}][e']}{[V_O^{\bullet}]} = K_{V_O^{1/2}}(T) = K^{\circ}_{V_O^{1/2}} \exp\left(\frac{-\Delta H_{V_O^{1/2}}}{k_B T}\right) \tag{41}$$

$\Delta H_{V_O^{0/1}}$ and $\Delta H_{V_O^{1/2}}$, according to experiment, are 3 meV and 0.3 eV, respectively.[47] In the band-structure picture, this corresponds to the levels lying just below the CB edge. Hence, they only become important under highly reducing conditions (as the Fermi level approaches the CB edge) at low temperatures.

Analogously, the ionization of strontium vacancies yields electron holes:

$$V_{Sr}^{\times} \rightleftharpoons V_{Sr}' + h^{\bullet} \tag{42}$$

$$V_{Sr}' \rightleftharpoons V_{Sr}'' + h^{\bullet} \tag{43}$$

with

$$\frac{[V_{Sr}'][h^{\bullet}]}{[V_{Sr}^{\times}]} = K_{V_{Sr}^{0/1}}(T) = K^{\circ}_{V_{Sr}^{0/1}} \exp\left(\frac{-\Delta H_{V_{Sr}^{0/1}}}{k_B T}\right) \tag{44}$$

$$\frac{[V_{Sr}''][h^{\bullet}]}{[V_{Sr}']} = K_{V_{Sr}^{1/2}}(T) = K^{\circ}_{V_{Sr}^{1/2}} \exp\left(\frac{-\Delta H_{V_{Sr}^{1/2}}}{k_B T}\right) \tag{45}$$

$\Delta H_{V_{Sr}^{0/1}}$ and $\Delta H_{V_{Sr}^{1/2}}$, according to experiment, are much deeper, being 0.1 eV and 1.4 eV, respectively, above the VB edge.[47] Acceptor dopant cations, too, have deep levels. The ionization reaction

$$Acc_{Ti}^{\times} \rightleftharpoons Acc_{Ti}' + h^{\bullet} \tag{46}$$

with equilibrium constant

$$\frac{[Acc_{Ti}'][h^{\bullet}]}{[Acc_{Ti}^{\times}]} = K_{Acc^{0/1}}(T) = K^{\circ}_{Acc^{0/1}} \exp\left(\frac{-\Delta H_{Acc^{0/1}}}{k_B T}\right) \tag{47}$$

exhibits $\Delta H_{Acc^{0/1}} > 1$ eV for Fe and Al.[40,46,49] In general, acceptor levels evidently lie deeper in the bandgap.

The other reaction that may take place in this low-temperature regime is the formation of dopant-vacancy associates

$$Acc_{Ti}' + V_O^{\bullet\bullet} \rightleftharpoons \{Acc_{Ti}' - V_O^{\bullet\bullet}\}^{\bullet}, \tag{48}$$

with equilibrium constant

$$\frac{[\{Acc_{Ti}' - V_O^{\bullet\bullet}\}^{\bullet}]}{[Acc_{Ti}'][V_O^{\bullet\bullet}]} = K_a(T) = K^{\circ}_a \exp\left(\frac{-\Delta H_a}{k_B T}\right) \tag{49}$$

The association energies are negative, are evidently some fraction of an eV and vary according to the acceptor dopant.[67–69] The total amount of dopant present in the system is thus divided into charged dopants, neutral dopants, and dopants in dopant–vacancy associates,

$$[Acc_{Ti}] = [Acc_{Ti}'] + [Acc_{Ti}^{\times}] + [\{Acc_{Ti}' - V_O^{\bullet\bullet}\}^{\bullet}] \tag{50}$$

5.2. Intermediate-Temperature Regime

Above $T \approx 750$ K, the kinetics of the oxygen exchange reaction become appreciable (k_O^s is sufficiently high),[46] such that the equilibrium between oxygen in the gas phase and oxygen in the solid can be established.[36,37,39,46,48] This can be written as the oxidation of the oxide,

$$\frac{1}{2}O_2(g) + V_O^{\bullet\bullet} \rightleftharpoons O_O^{\times} + 2h^{\bullet} \tag{51}$$

or as the reduction of the oxide,

$$O_O^{\times} \rightleftharpoons \frac{1}{2}O_2(g) + V_O^{\bullet\bullet} + 2e' \tag{52}$$

These are not independent reactions, however. Equation (51), for example, can be obtained by combining Eqs. (52) and (35). The equilibrium constant of the reduction reaction is given by

$$\frac{[V_O^{\bullet\bullet}][e']^2 a O_2^{1/2}}{[O_O^{\times}]} = K_{red}(T) = K^{\circ}_{red} \exp\left(\frac{-\Delta H_{red}}{k_B T}\right) \tag{53}$$

with reduction enthalpies reported in the literature in the range of $\Delta H_{red} = 5$–6 eV.[46,47,59]

For the sake of completeness I also mention that oxygen vacancies not only react with oxygen (see above) but also react with water to generate substitutional hydroxide groups,[42–44]

$$H_2O(g) + O_O^{\times} + V_O^{\bullet\bullet} \rightleftharpoons 2OH_O^{\bullet} \tag{54}$$

the equilibrium constant for this hydration reaction is

$$\frac{[OH_O^{\bullet}]^2}{[V_O^{\bullet\bullet}][O_O^{\times}] a H_2O} = K_{hyd}(T) = K^{\circ}_{hyd} \exp\left(\frac{-\Delta H_{hyd}}{k_B T}\right) \tag{55}$$

Values of the hydration enthalpy, ΔH_{hyd}, from experiment and theory vary from –0.24 eV to –0.72 eV.[42,43,70,71] Although the kinetics of water vapor incorporation into $SrTiO_3$ have not received the attention that oxygen incorporation kinetics have, one may expect that water incorporation is faster. It is conceivable, therefore, that water may be incorporated into

acceptor-doped $SrTiO_3$ at temperatures at which oxygen incorporation is negligible.

5.3. High-Temperature Regime

Finally, at temperatures above $T = 1300$ K, strontium vacancies display sufficient mobility,[51,72] such that the partial Schottky disorder reaction,

$$Sr_{Sr}^{\times} + O_O^{\times} \rightleftharpoons V_{Sr}'' + V_O^{\cdot\cdot} + SrO(s) \quad (56)$$

becomes active. The enthalpy of SrO partial Schottky disorder, defined according to

$$\frac{[V_{Sr}''][V_O^{\cdot\cdot}]a\mathrm{SrO}}{[O_O^{\times}][Sr_{Sr}^{\times}]} = K_{Sch}(T) = K_{Sch}^{\circ}\exp\left(\frac{-\Delta H_{Sch}}{k_B T}\right) \quad (57)$$

was determined experimentally to be $\Delta H_{Sch} = 2.5$ eV.[47] Theoretical estimates of ΔH_{Sch} are at least 1 eV higher (see Ref.[57] and references therein): The reason for this discrepancy is unknown.

5.4. Bringing it All Together

In its fullest form, the charge neutrality for acceptor-doped $SrTiO_3$ can therefore be written as

$$[e'] + [Acc_{Ti}'] + [V_{Sr}''] + 2[V_{Sr}''] = [h^{\cdot}] + [V_O^{\cdot}] + 2[V_O^{\cdot\cdot}] + [OH_O^{\cdot}] + [\{Acc_{Ti}'\text{-}V_O^{\cdot\cdot}\}^{\cdot}] \quad (58)$$

that is, there are nine charged point defects: electrons, charged acceptor dopants, singly and doubly charged strontium vacancies, electron holes, singly and doubly charged oxygen vacancies, hydroxide ions and dopant–vacancy associates. In addition, there are neutral acceptor dopants, neutral strontium vacancies and neutral oxygen vacancies. In order to obtain all twelve defect concentrations in the high-temperature regime, one must solve twelve equations simultaneously (electroneutrality, mass conservation of the dopant, and ten defect equilibria), having specified the thermodynamic variables, $[Acc_{Ti}]$, aO_2, aH_2O, $a\mathrm{SrO}$, and T. Under certain conditions, however, one finds that various defect concentrations are negligibly small, and hence that the associated defect reactions are of little importance. For example, in the high and intermediate temperature regimes, oxygen vacancies and strontium vacancies are fully ionized, and dopant–vacancy pairs are fully dissociated; hence the ionization reactions and the association reactions do not need to be taken into account. Furthermore, under dry conditions, $[OH_O^{\cdot}]$ is negligibly small; thus, the hydration reaction is of minor importance, and aH_2O does not need to be considered as a thermodynamic variable. As a consequence, the full electroneutrality condition can be simplified, in the high- and intermediate-temperature regimes, to

$$[e'] + [Acc_{Ti}'] + 2[V_{Sr}''] = [h^{\cdot}] + 2[V_O^{\cdot\cdot}] \quad (59)$$

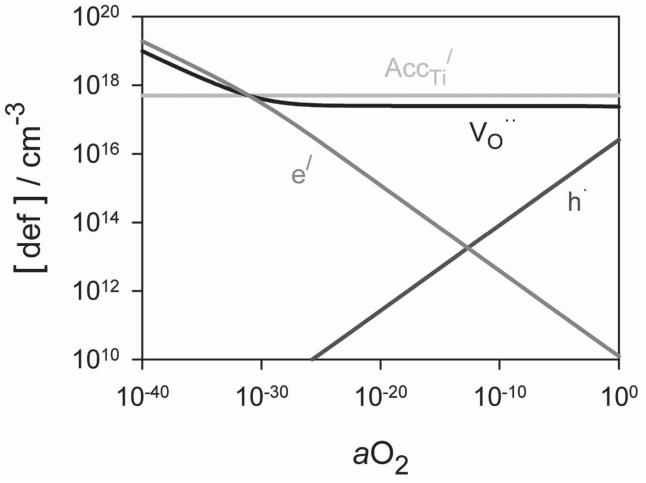

Figure 5. Point-defect concentrations in acceptor-doped $SrTiO_3$ ($[Acc'_{eff}] = 5 \times 10^{17}$ cm^{-3}) predicted by defect-chemical modelling as a function of oxygen activity aO_2 at a temperature of $T = 900$ K (intermediate-temperature regime).

The number of defect equilibria that now need to be taken into account to obtain these defect concentrations still depends, as already noted above, on the temperature. Let us consider the following experiment. A sample of acceptor-doped $SrTiO_3$ is held at $T = 1400$ K, $aO_2 = 0.2$, $a\mathrm{SrO} = 1$ to attain equilibrium. There are four unknowns, and thus one needs to solve four equations, Equations (36), (53), (57), and (59), simultaneously (for the given thermodynamic variables $[Acc_{Ti}]$, aO_2, $a\mathrm{SrO}$, and T).

Let us now quench the equilibrated sample to $T = 900$ K. Since V_{Sr}'' are not sufficiently mobile at this lower temperature, $[V_{Sr}'']$ cannot change from the high temperature value. Consequently, in this intermediate-temperature regime, $[V_{Sr}'']$ is a constant (the defects are frozen-in, and act effectively as additional acceptors), $a\mathrm{SrO}$ is no longer a relevant thermodynamic variable, and there are only three equations to be solved for three unknowns with three thermodynamic variables. Exemplary results are shown in **Figure 5** for a total acceptor concentration, $2[V_{Sr}''] + [Acc_{Ti}'] = [Acc_{eff}'] = 5 \times 10^{17}\,\mathrm{cm}^{-3}$. At this temperature and for this acceptor concentration, one discerns that the defect chemistry is generally governed by the acceptor species, that is, $[Acc_{eff}'] = 2[V_O^{\cdot\cdot}] > [h^{\cdot}], [e']$. Only under the most reducing conditions ($aO_2 < 10^{-32}$ for this T and $[Acc_{eff}']$) does the electroneutrality condition become $2[V_O^{\cdot\cdot}] = [e']$.

Having equilibrated the sample at this temperature ($T = 900$ K) and this oxygen activity ($aO_2 = 0.2$), we now quench the sample to $T < 550$ K. The limited surface reaction kinetics prevent the concentration of oxygen vacancies in the sample from adjusting to the new conditions. Hence, $[V_O^{\cdot\cdot}]$ is now also constant (fixed at the value from the quenching temperature), and aO_2 is no longer a relevant thermodynamic variable. The ionization reactions and dopant–vacancy association may, however, become important.[45,73,74] For the purpose of illustration, let us assume that only the ionization reaction of an acceptor species $Acc_{Ti}^{\times}$ becomes important. In this case, there are four equations, Equations (36), (47), (50), and (59), to be solved for four unknowns with two thermodynamic variables.

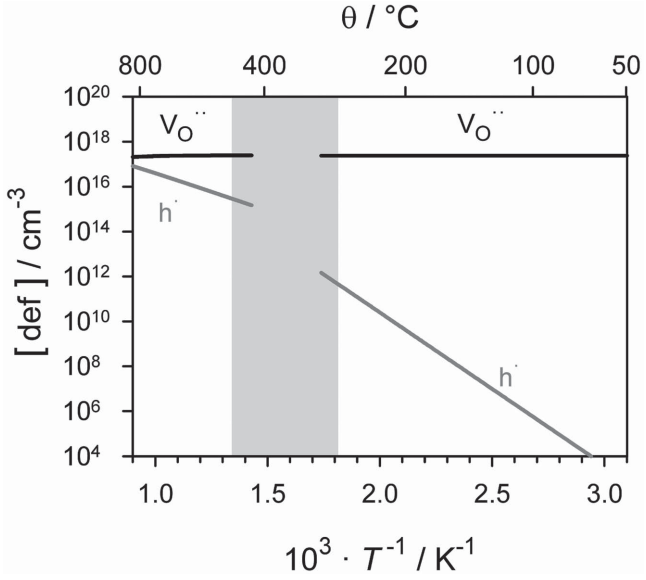

Figure 6. Concentrations of mobile point defects in acceptor-doped $SrTiO_3$ ([Acc'_{eff}] = 10^{18} cm^{-3}) predicted by defect-chemical modelling as a function of temperature for the intermediate-temperature and low-temperature regimes (see text).

In **Figure 6**, the concentrations of oxygen vacancies and electron holes are plotted in the intermediate-temperature and low-temperature regimes. No data are plotted for the shaded region, denoting 750 ≥T/K ≥ 550, because the surface reaction is so slow that a macroscopic sample would not reach equilibrium in a reasonable time (months to years) but not so slow that the sample's oxygen content does not change significantly with time. It is emphasised that, although their concentration is fixed, oxygen vacancies are still mobile in this low-temperature regime. The surface shuts the sample off from the surroundings, but this doesn't, indeed it cannot, affect the vacancy mobility. This has important consequences for the measured conductivity (see Section 6.2).

6. Diffusion Experiments Applied to $SrTiO_3$

The renowned physical chemist W. Oswald noted in 1891 that, "To make accurate experiments on diffusion is one of the most difficult problems in practical physics." This is particularly true of $SrTiO_3$. In this section, some of the complications that one encounters in studying oxygen diffusion in this material are discussed.

6.1. Tracer Diffusion

Oxygen isotope diffusion profiles measured for nominally undoped $SrTiO_3$ single crystals display two features:[32,58,75] a sharp drop over tens of nanometers close to the surface followed by a shallow decrease extending several micrometers into the solid. The first feature can be assigned to a surface space-charge layer depleted of oxygen vacancies; the second feature, to diffusion in a homogeneous bulk phase. The entire profile can be described by a single solution to the diffusion equation [Equation (3)] that includes isotope transport across a gas|solid interface, through a space-charge layer depleted of oxygen vacancies, and into a bulk phase of uniform vacancy concentration (**Figure 7**). The description yields the tracer diffusion coefficient in the bulk D_O^*, the surface exchange coefficient k_O^* and the surface space-charge potential Φ_0.

The traditional interpretation of such two-feature profiles ascribes the first feature to bulk diffusion and the second feature to a combination of fast diffusion along dislocations (with diffusion coefficient $D_O^{*,dis}$) and diffusion out of the dislocations (with diffusion coefficient D_O^*). This is known as Harrison type B diffusion kinetics.[2,10,76]

In the case of acceptor-doped $SrTiO_3$, however, this interpretation can be excluded for a number of reasons. First, increasing the dopant concentration causes the extent of the first feature to decrease but the extent of the second feature to increase (compare isotope profiles reported in Refs.[58,75]: this is consistent with the first feature arising from a depletion space-charge zone and the second feature arising from bulk diffusion. Second, the evolution of the experimentally measured profiles as a function of time is consistent with space-charge layers but not with grain boundary diffusion.[77] Third, analysis of the diffusion coefficients obtained from the second feature yields oxygen-vacancy diffusivities that are consistent with values obtained independently for the bulk phase by a variety of other methods (see discussion in Section 6.4). Fourth, the activation enthalpy for vacancy migration in the bulk phase obtained from the analysis is in excellent accord with values from other experimental and theoretical studies (see Sec. 6.4). Fifth, both features are reproducible. Within experimental error, they do not vary across a sample nor from sample to sample. This implies that the behavior is characteristic of $SrTiO_3$ as a thermodynamic system, and thus militates strongly against the dislocation interpretation. Sixth, a depletion space-charge layer is expected on thermodynamic grounds to be present at a surface. Extensive work on grain boundaries in $SrTiO_3$ has indicated the

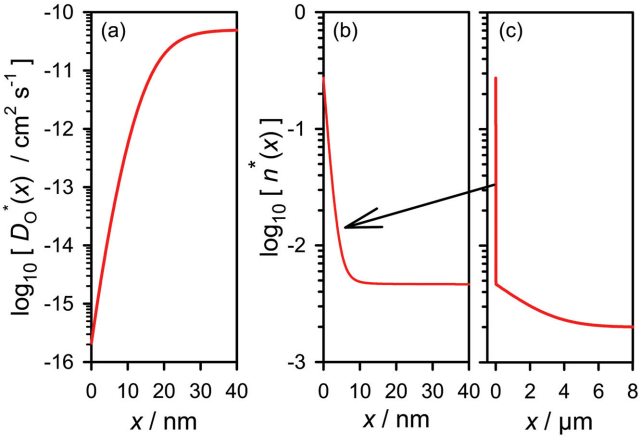

Figure 7. Isotope transport through an equilibrium surface space-charge layer depleted of oxygen vacancies.[32,58,75] a) Local variation of the oxygen tracer diffusion coefficient, $D_O^*(x) = f^* D_V n_V(x) \approx D_O^*(\infty)\exp[-2e\phi(x)/k_BT]$, that arises from oxygen-vacancy depletion near the surface. Solving Equation (3) with this spatially variant $D_O^*(x)$ yields the isotope profile shown in b) [the first 40 nm], and in c) [the entire profile].

presence of depletion space-charge layers (see Refs.[33,78] and references therein). Considering a surface simplistically as half a grain boundary, one would expect a surface space-charge layer to be present.

It is also pointed out that isotope profiles with two features have also been observed for analogous perovskite-oxide compositions: $Pb(Zr,Ti)O_3$,[79,80] $BaTiO_3$,[81] $LaAlO_3$,[82] and possibly $CaTiO_3$[83] (see also Section 6.5).

6.2. Conductivity

Determining the oxygen-ion conductivity of acceptor-doped $SrTiO_3$ is not simple. In the high- and intermediate-temperature regimes, the conductivity is predominantly electronic, because the mobilities of electrons and of holes are orders of magnitude higher than that of oxygen vacancies (with strontium vacancies being less mobile still): $u_{e'} \sim u_{h^\cdot} \gg u_{V_O^{\cdot\cdot}} \gg u_{V_{Sr}''}$.[47,58,72] Starting with the defect concentration shown in Figure 5, and multiplying by the respective charges and defect mobilities, one obtains the classical V-form that corresponds to *p*-type conductivity at high oxygen activities [with $\sigma \propto (aO_2)^{+1/4}$] and to *n*-type conductivity at low oxygen activities [with $\sigma \propto (aO_2)^{-1/4}$]. **Figure 8** is a plot of the measured conductivity of a nominally undoped $SrTiO_3$ single crystal as a function of oxygen activity at three temperatures.[32,59] The partial ionic conductivity is apparent at the lowest temperature, as an aO_2-independent term that results in a flattened minimum. At the higher temperatures, the ionic contribution is swamped by the electronic contributions. One could consider this as the point-defect behavior preventing the determination of the ionic conductivity.

In the low-temperature regime, however, the point-defect behavior allows the ionic conductivity to be determined directly.[45,74] The experiment makes use of the fact that the concentration of electron holes is strongly diminished in a sample equilibrated in oxidising conditions and $T > 750$ K and then quenched to $T < 550$ K. The acceptor-like defects (acceptor dopants but also strontium vacancies) trap the electron holes, drastically reducing the *p*-type conductivity. Using the defect concentrations of Figure 6 and defect mobilities,[47,58] one can predict the partial conductivities in the intermediate- and low-temperature regimes. One recognises in **Figure 9**(a) that electron holes provide the dominant contribution to the conductivity in the former regime, but in the quenched state, it is oxygen vacancies. Figure 9(b) shows three sets of experimental data.[84–86] In the original studies, the measured conductivity was ascribed to either electron holes[84,85] or to singly and doubly charged vacancies.[86] The comparison with (a) clearly indicates that the correct assignment is doubly charged vacancies at low temperatures and electron holes at higher temperatures. In addition, the activation enthalpies of the conductivity predicted

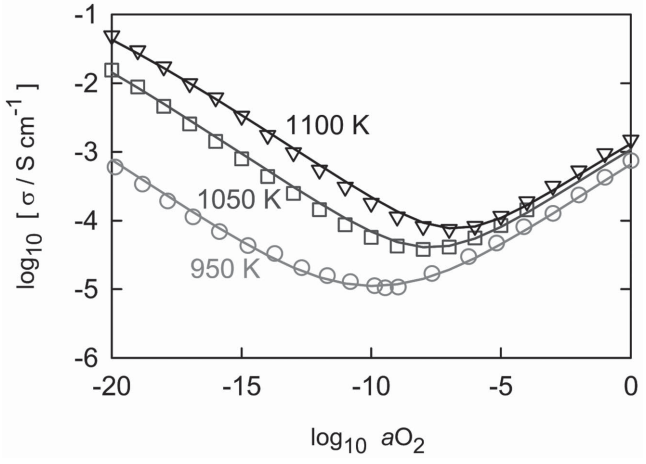

Figure 8. Equilibrium conductivity of nominally undoped (weakly acceptor doped) $SrTiO_3$ as a function of oxygen activity aO_2 at three temperatures in the intermediate-temperature regime. Symbols are experimental data; lines are predictions from defect-chemical modelling.[32,59]

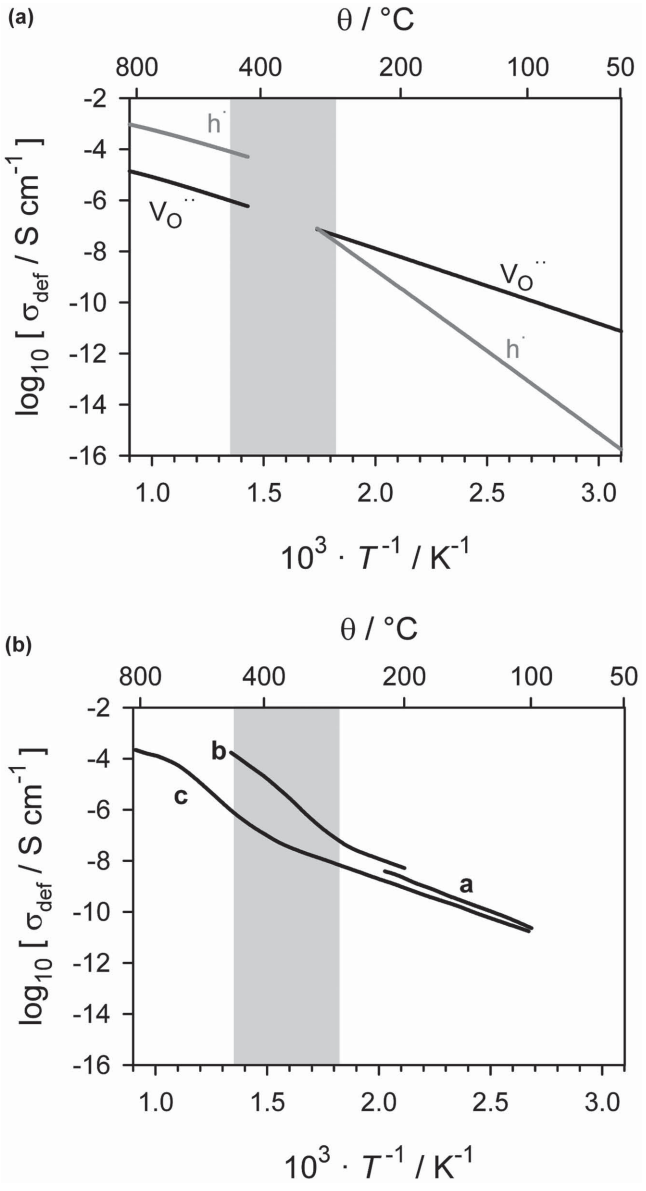

Figure 9. Conductivity of nominally undoped (weakly acceptor doped) $SrTiO_3$ as a function of temperature (under oxidising conditions). a) Predicted conductivity in the intermediate-temperature (equilibrium) and low-temperature (quenched) regimes. b) Experimentally measured conductivity: **a**[84] **b**[85] **c**[86].

for the intermediate- and low-temperature regimes are in excellent agreement with measured values from Wang et al.,[86] namely 0.49 eV in the intermediate regime and 0.6 eV in the low-temperature regime. Note, too, that the conductivity measured in the transition region will vary depending on how fast the measurements were performed, and whether they were performed from high temperatures downwards or from low temperatures upwards (hysteresis is to be expected).

6.3. Chemical Diffusion

The two best properties that can be used to follow chemical diffusion in acceptor-doped $SrTiO_3$ are conductivity[87,88] and color.[26,27,89] The former requires the application of electrodes, which obviously entails covering (at least part of) the free surface and introducing a different interface between the electrode and $SrTiO_3$. The latter requires a dopant species that changes its valence and thus its absorption band in the appropriate window of temperature and oxygen activity; Fe is such a dopant.[40] Since in general macroscopic samples are used, the effect of the depletion space-charge layer may only be apparent at very short times in relaxation experiments.[90]

The analysis of chemical diffusion data is easiest in the defect regime, $[e'] = 2[V_O^{\cdot\cdot}]$, for which Equation (26) is valid. At high oxygen activities, the presence of a variable-valence dopant, such as Fe, requires a more complicated analysis[6,26,27] that nevertheless may yield Equation (26) in the end.

6.4. Summary for $SrTiO_3$

Comparison of diffusion data is done best at the level of defect diffusion coefficients, D_{def}. The benefit for systems in which the interactions between point defects are negligible is, as noted previously, that the defect diffusion coefficients are independent of defect concentration; at high defect concentrations, D_{def} is generally expected to vary with defect concentration. Extracting D_{def} from measured D^*, D^δ, or D^σ does require, however, detailed knowledge of the defect chemistry; as we will see, this is not always available.

In **Figure 10** data determined for the diffusivity of $V_O^{\cdot\cdot}$ in $SrTiO_3$ are summarised. Chemical diffusion measurements yielded datasets **a**, **b**, **c** and **d**;[87,88,91,92] electrical measurements yielded **e**, **f**, **g** and **k**[45,84,86,93] an acceptor level of 5×10^{17} cm^{-3} was assumed to convert conductivities of nominally undoped single crystals into vacancy diffusion coefficients); and tracer diffusion studies yielded the dataset **h**. The global expression **j** was derived in Ref.[58] to describe **a**, **h** and **e**; it is seen here to describe additional data **c**, **d**, **f** and **g** as well. This good agreement extends the range of the global expression down to room temperature and confirms its reliability.

Concerning the activation enthalpy of vacancy migration, one satisfyingly finds good agreement between macroscopic

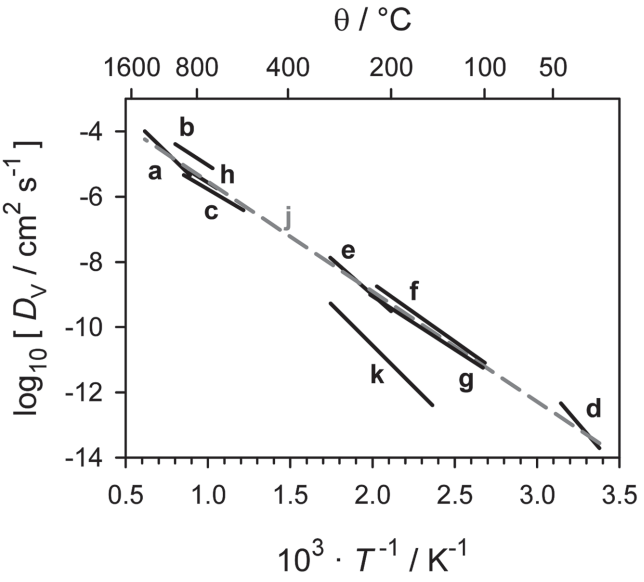

Figure 10. Comparison of vacancy diffusion coefficients obtained experimentally for $SrTiO_3$. **a**[91] **b**[87] **c**[88] **d**[92] **e**[93] **f**[84] **g**[86] **h**[58] **j**, global expression derived in previous work[58] **k**[45].

(chemical,[87] tracer,[58] conductivity[84,86] diffusion experiments; microscopic (nuclear spin relaxation[94] and anelastic relaxation[95] hopping experiments; and atomistic simulations.[32,96,97] The value is in the range of $\Delta H_{mig,V_O^{\cdot\cdot}} = 0.62 - 0.67$ eV.

At lower temperatures, defect interactions involving oxygen vacancies evidently become important. There is experimental evidence that acceptor-dopant cations, such as Ni_{Ti}'',[45] Mn_{Ti}'[67,68] and Fe_{Ti}',[67,68] trap oxygen vacancies at nearest-neighbor positions. A recent computational study[69] revealed that the dopant cation affects the site energies of a vacancy beyond the nearest-neighbor position, and furthermore, it increases the local activation energies for vacancy motion, as indicated in **Figure 11**. The consequence for the long-range migration of oxygen vacancies is an increase in the measured activation enthalpy of diffusion or conduction. In the case of Ni-doped $SrTiO_3$ (**k** in Figure 10), for example, the measured activation enthalpy, from conductivity investigations, increases to ca. 1 eV.[45] Not all acceptor-dopant species cause a change in activation enthalpy, however: the interactions are evidently negligible

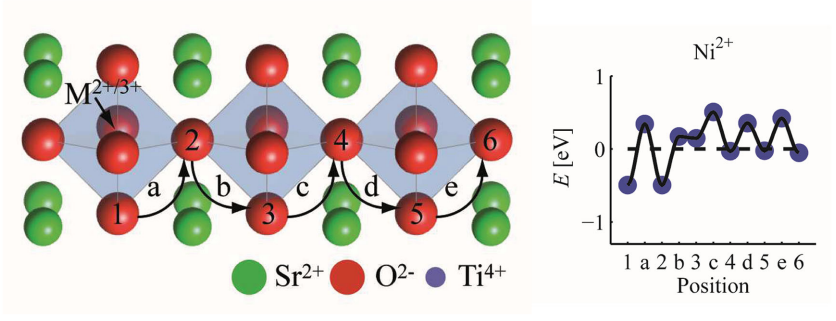

Figure 11. Schematic illustration (left) and corresponding energy landscape (right) of an oxygen vacancy around an acceptor dopant Ni_{Ti}'' in $SrTiO_3$. The positions 1 to 6 refer to site energies, whereas the positions a to denote saddle-point energies.[69]

in the case of nominally undoped $SrTiO_3$ (**j** in Figure 10), with the migration enthalpy remaining constant down to room temperature.[84,86,98]

6.4.1. Diffusion Across and Along Extended Defects

Grain boundaries in acceptor-doped $SrTiO_3$ and $BaTiO_3$, that are free of second phases, are found universally to display lower conductivities (for transport across the interfaces) than that of the bulk phase. This behavior can be accounted for quantitatively in terms of positively charged grain boundaries and negatively charged space-charge layers.[33,78] There is currently no evidence for fast transport of oxygen along grain boundaries or dislocations. Schaffrin, in a chemical diffusion experiment,[99] and Watanabe et al., in a tracer diffusion experiment,[100] found polycrystalline samples to behave as indicated in Figure 4a, and thus observed drops in oxygen (concentration/isotope) profiles at grain boundaries, as indicated in Figure 4b. (See also the study by Leonhardt et al. for chemical diffusion experiments on a bicrystal.)[101] No preferential penetration of oxygen along grain boundaries was observed in either case.

There are several reports of fast-path diffusion of oxygen along dislocations in $SrTiO_3$,[91,102–105] but in all cases there are doubts concerning not only how the work was performed, but also how the results were analysed and interpreted. A recent experimental study found no evidence for the fast diffusion of oxygen along edge dislocations comprising a low-angle tilt grain boundary.[32] In addition, static lattice calculations indicated a thermodynamic driving energy for space-charge formation at edge dislocations, confirming earlier predictions,[33,106] and tentatively concluded that the activation barriers for oxygen ion migration were higher at dislocations than in the bulk. Molecular dynamics simulations of oxygen diffusion along the grain boundary confirm that diffusion along the dislocations is slower than in the bulk.[107] It appears that in oxide systems, in which one ion is highly mobile in the bulk phase (for example, oxygen ions in perovskite-structured oxides and in fluorite-structured oxides), ion transport along extended defects in hindered.[32,108,109]

6.5. Oxygen Diffusion in Related Titanate Perovskite Oxides

There is more than one set of oxygen diffusion data for each of $BaTiO_3$ (BT), $CaTiO_3$ (CT), and $Pb(Zr,Ti)O_3$ (PZT). The extensive data available for $BaTiO_3$ are discussed in detail elsewhere.[81] In this section data for nominally undoped $CaTiO_3$ and $Pb(Zr,Ti)O_3$ are reviewed, in order to draw attention to certain problems and discrepancies.

Figure 12 is a summary of oxygen self-diffusion coefficients for $CaTiO_3$[83,110–112] and $Pb(Zr,Ti)O_3$.[79,80,113] Given the available data and the lack of knowledge concerning the effective acceptor concentrations in the samples that were studied, it was deemed prudent to consider D_O rather than $D_{V_O^{\cdot\cdot}}$. Where tracer data are available, self-diffusion coefficients were calculated with the tracer correlation coefficient for a cubic ABO_3 perovskite ($f^* = 0.69$[28], even though CT[114] and PZT[115] do not exhibit cubic symmetry throughout the entire range of investigated temperatures. Chemical diffusion data (available

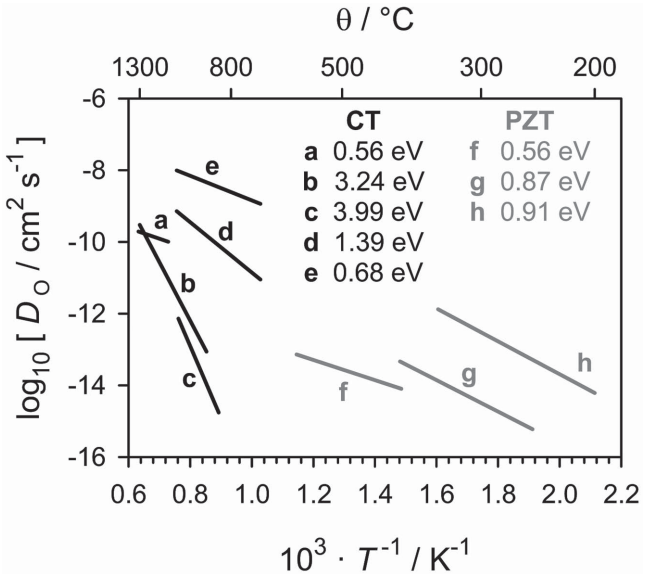

Figure 12. Comparison of oxygen self-diffusion coefficients obtained experimentally for $CaTiO_3$ (**a**[110] **b**[111] **c**[83] **d**[112] **e**[112] and $Pb(Zr,Ti)O_3$ (**f**[79] **g**[80] **h**[113].

for CT) were converted via vacancy diffusion coefficients into self-diffusion coefficients on the assumptions of $D_{V_O^{\cdot\cdot}} = D_O^{\delta}/3$ and $[Acc'] = 2 \times 10^{19}$ cm^{-3}. Since some of the CT specimens studied were taken from the naturally occurring mineral, considerable variation between oxygen self-diffusion coefficients is to be expected.

Nevertheless, examination of the data for CT in Figure 12 does not yield a consistent picture. The activation enthalpies of self-diffusion, in particular, vary from 0.56 eV to 4 eV. The problem may be due in part to the tracer data: Gautason and Muehlenbachs[111] conducted gas-phase monitoring of isotope exchange, but did not take account of surface exchange kinetics, which probably determined the overall rate of exchange for their powder samples. Sakaguchi and Haneda,[83] in contrast, obtained isotope profiles in the solid—isotope profiles with two features—, but they attributed the first feature to bulk diffusion and the second to fast-diffusion along twin boundaries. It is unclear whether this traditional assignment, or whether the alternative—diffusion through a depletion space-charge layer followed by bulk diffusion (see Section 6.1)—is correct.

In the case of PZT, the data may be consistent at the level of the vacancy diffusivity. Differences in the absolute magnitude of D_O may arise from the slightly different formal compositions, $Pb(Zr_{0.35}Ti_{0.65})O_3$,[79] $Pb(Zr_{0.4}Ti_{0.6})O_3$,[80] and $Pb(Zr_{0.5}Ti_{0.5})O_3$;[113] and from the differing degrees of lead deficiency, in view of the electroneutrality condition being $2[V_{Pb}''] = 2[V_O^{\cdot\cdot}]$.[116] Consequently, this suggests that at the investigated (low) temperatures, $[V_{Pb}'']$ is constant, which fixes $[V_O^{\cdot\cdot}]$, and hence that $\Delta H_{gen,V_O^{\cdot\cdot}}$ is zero. Consequently, the measured activation enthalpy of oxygen diffusion refers to migration alone. The data do imply a change in migration enthalpy, from 0.9 eV to 0.6 eV at around 400 °C, coincident with the change in symmetry to the high-temperature cubic structure.[115] Further studies of D_O^* (and D_{Pb}^*!) will prove helpful in elucidating the migration behavior of point defects in this material.

It is emphasised that, in both oxygen tracer diffusion studies of PZT,[79,80] a sharp feature in the isotope profile at the surface was observed. And in both cases it was assigned to the presence of a space-charge layer depleted of mobile oxygen vacancies.

6.6. Oxygen Diffusion in Related Zirconate and Cerate Perovskite Oxides

The examination of oxygen-ion transport in the alkaline-earth zirconate perovskites [$CaZrO_3$ (CZ), $SrZrO_3$ (SZ), $BaZrO_3$ (BZ)] and cerate perovskites [$SrCeO_3$ (SC), $BaCeO_3$ (BC)] is complicated by three factors. First, and most importantly, these materials dissolve significant amounts of water according to Eq. (54), generating high concentrations of mobile protons.[43,128–131] The measured conductivity may contain contributions, therefore, from electrons, electron holes, oxygen vacancies and protons. And a conductivity that is independent of aO_2, though free of electronic contributions, may be due to oxygen vacancies or protons, or some mixture thereof.

Second, the materials that have been investigated are not dilute systems but solid solutions: the host Zr^{4+} or Ce^{4+} is substituted with, say, 10% or more of Y^{3+}, In^{3+}, or Gd^{3+}. This may lead to the vacancy diffusivity varying with the amount and type of trivalent substituent, on account of defect interactions and/or changes in crystal symmetry. Third, the effective concentration of acceptors (and thus that of oxygen vacancies) may be much lower than the nominal value, because the trivalent cations may substitute onto both divalent *A* sites (and act as donors) and tetravalent *B* sites (and act as acceptors);[43,131] in addition, the trivalent cations may possess limited solubility (for a nominal 10% substitution of In^{3+} into CZ, only ≈4% is incorporated into the CZ lattice[128].

Bearing these points in mind, let us consider the data plotted in **Figure 13** for the alkaline-earth zirconates. Here I have not attempted a comprehensive review of the literature; rather I present selected data that are probably representative of oxygen-vacancy diffusion (it is difficult to be certain if one only has conductivity data to hand). The (pseudo-)cubic BZ and SZ compositions display relatively similar values of D_V, whereas the strongly distorted (orthorhombic) CZ compositions show considerably lower values. The activation enthalpies of vacancy migration behave correspondingly, with BZ[43,117–119,132,133] and SZ[43,120–122] solid solutions exhibiting $\Delta H_{mig,V} \approx 1$ eV, whilst those for CZ are much higher, varying from 1.8 eV up to 2.6 eV.[123–127]

Figure 14 compares oxygen-vacancy diffusivities in solid solutions based on the alkaline-earth cerate perovskites: $BaCeO_3$ (BC)[43,134–136] and $SrCeO_3$ (SC).[43,124,137] The datasets **a**, **b**, and **c** all refer to $BaCe_{0.9}Y_{0.1}O_{2.95}$; they agree very well with one another and they can be described with a single activation enthalpy of 0.62 eV. The single crystal data, **d**, has a lower vacancy diffusivity and a higher activation enthalpy of migration, both of which may arise from the different dopant (Gd) or from the supposed distribution of Gd on both cation sites [$(Ba_{0.98}Gd_{0.02})(Ce_{0.87}Gd_{0.13})O_{2.945}$].[136] In comparison, the D_V values for SC are significantly lower, and this can be attributed to SC adopting a more distorted structure (orthorhombic) than BC (pseudo-cubic). Surprisingly, the two oxygen tracer diffusion studies (**e**[124] and **g**[137]) on SC with 5% Yb show some

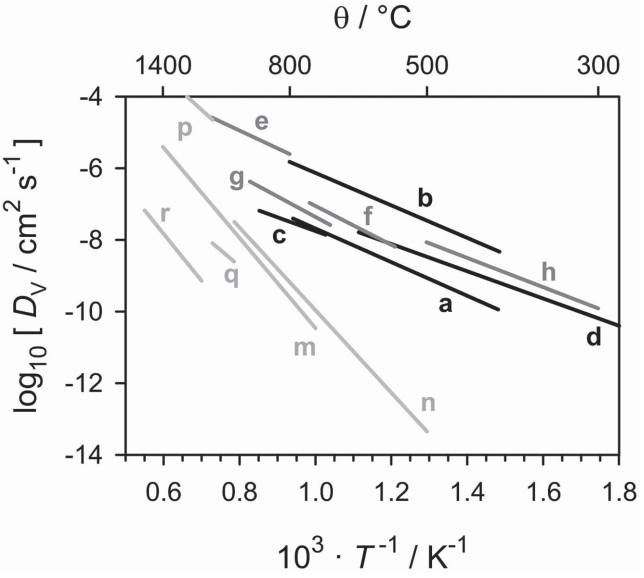

Figure 13. Comparison of oxygen-vacancy diffusion coefficients obtained experimentally from conductivity studies for solid solutions based on $A^{II}ZrO_3$ perovskites. $BaZrO_3$: **a**[43] **b**[117] **c**[118] **d**[119]. $SrZrO_3$: **e**[120] **f**[121] **g**[43] **h**[122]. $CaZrO_3$: **m**[123] **n**[124] **p**[125] **q**[126] **r**[127].

differences, but are of a similar order of magnitude to data (**f**[43]) extracted from conductivity measurements.

Comparing, finally, data from titanates, zirconates and cerates, one finds that the highest vacancy diffusivities are found for weakly acceptor-doped $SrTiO_3$ and $BaCe_{0.9}Y_{0.1}O_{2.95}$ (with almost identical activation enthalpies and pre-exponential factors), and the lowest for $CaZr_{0.96}In_{0.04}O_{2.98}$. In general, strong distortions of the perovskites structure will lead to lower diffusivities for oxygen vacancies.

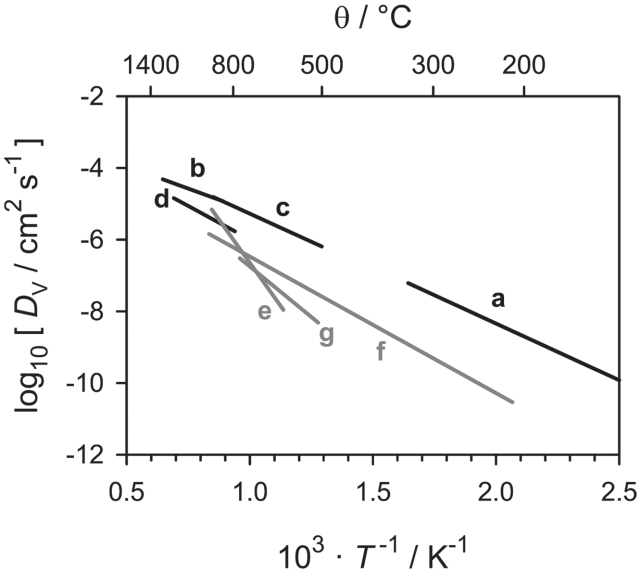

Figure 14. Comparison of oxygen-vacancy diffusion coefficients obtained experimentally for selected solid solutions based on $A^{II}CeO_3$ perovskites. $BaCeO_3$: **a**[43] **b**[134] **c**[135] **d**[136]. $SrCeO_3$: **e**[124] **f**[43] **g**[137].

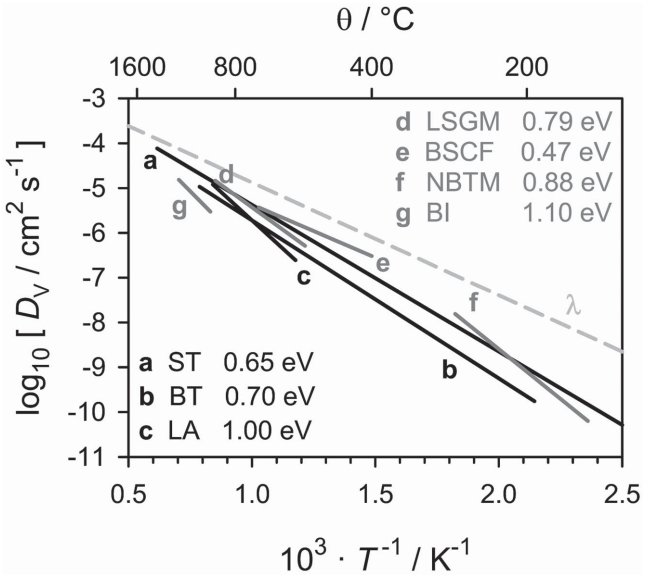

Figure 15. Comparison of oxygen-vacancy diffusion coefficients obtained experimentally for selected perovskite oxides. **a**:[58] $SrTiO_3$; **b**:[81] $BaTiO_3$; **c**:[82] $LaAlO_3$; **d**:[138] $(La_{0.9}Sr_{0.1})(Ga_{0.9}Mg_{0.2})O_{2.85}$; **e**:[139] $(Ba_{0.5}Sr_{0.5})(Co_{0.8}Fe_{0.2})O_{3-\delta}$; **f**:[140] $(Na_{0.50}Bi_{0.49})(Ti_{0.98}Mg_{0.02})O_{2.965}$; **g**:[141] $BaInO_{2.5}$; and λ, prediction from Equation (60), see text.

7. The Diffusion of Oxygen Vacancies in ABO_3 Perovskite Oxides

By way of concluding this article, I compare in **Figure 15** the diffusion coefficient for oxygen vacancies in selected $A^{II}B^{IV}O_3$ perovskites, $A^{III}B^{III}O_3$ perovskites, and one disordered $A^{II}B^{III}O_{2.5}$ brownmillerite. In addition to data for three nominally undoped (weakly acceptor-doped) systems, $SrTiO_3$,[58] $BaTiO_3$[81] and $LaAlO_3$,[82] data for four highly defective perovskite oxides are plotted: $(La_{0.9}Sr_{0.1})(Ga_{0.9}Mg_{0.2})O_{2.85}$ LSGM,[138] $(Ba_{0.5}Sr_{0.5})(Co_{0.8}Fe_{0.2})O_3.\delta$ BSCF,[139] $(Na_{0.50}Bi_{0.49})(Ti_{0.98}Mg_{0.02})O_{2.965}$ NBTM,[140] and $BaInO_{2.5}$ BI.[141] LSGM and NBTM constitute two of the best perovskite-based oxygen-ion electrolytes; BSCF is, perhaps, the best mixed conducting (electronic and oxygen-ionic) perovskite oxide. The data plotted for BI refer to the high-temperature phase, in which the oxygen vacancies are randomly distributed, and not to the low-temperature brownmillerite phase with ordered vacancies.

It is extremely surprising, therefore, to find that, regardless of vacancy site fraction, the oxygen-vacancy diffusivity for ST, BT, LA, LSGM, BSCF, NBTM, and BI all lie very close together in Figure 15. Does this indicate a fundamental limit to the oxygen-vacancy diffusivity in an ABO_3 perovskite? Although it is impossible to reach any firm conclusion at present, one can try to estimate a limit for $D_{V_O^{\cdot\cdot}}$. From Equation (18) one can express the vacancy diffusivity in terms of five quantities, namely,

$$D_{V_O^{\cdot\cdot}}(T) = \frac{1}{6}a^2 Z \nu_0 \exp\left(\frac{\Delta S_{\mathrm{mig},V_O^{\cdot\cdot}}}{k_B}\right)\exp\left(\frac{-\Delta H_{\mathrm{mig},V_O^{\cdot\cdot}}}{k_B T}\right) \quad (60)$$

Three of the five quantities are relatively certain. For a perovskite oxide that is cubic (all sites and jump distances are equivalent) and that has a unit-cell length 4.25 Å, one has $Z = 8$ and $a = 3.01$ Å. Also, $\Delta H_{\mathrm{mig},V_O^{\cdot\cdot}}$ is evidently at least 0.5 eV.[15–17,28] The two remaining quantities are problematic, or rather, the term $\nu_0 \exp(\Delta S_{\mathrm{mig},V_O^{\cdot\cdot}}/k_B)$ is problematic. If one takes the attempt frequency to be of the order of the Debye frequency $\nu_0 \approx 10^{13}$ Hz, and if one assumes, for the sake of argument, $\Delta S_{\mathrm{mig},V_O^{\cdot\cdot}} = -k_B$, one obtains the line λ in Figure 15. (Activation entropies of vacancy migration are not known for perovskites but for simple ionic solids they are ± a few k_B.)[6]

Evidently, if the activation entropy of vacancy migration for various perovskite oxides is generally not higher than $-k_B$ (for $\nu_0 = 10^{13}$ Hz), then we are already at or close to the physical limit of $D_{V_O^{\cdot\cdot}}$. If, on the other hand, the activation entropy of vacancy migration is much higher (and one requires $\Delta S_{\mathrm{mig},V_O^{\cdot\cdot}} = +3.6k_B$ for an increase in $D_{V_O^{\cdot\cdot}}$ of 10^2), then obviously perovskite oxides with superior vacancy diffusivities are waiting to be discovered. Whether it is physically possible to combine, in one material, high a, high $\nu_0 \exp(\Delta S_{\mathrm{mig},V_O^{\cdot\cdot}}/k_B)$ and low $\Delta H_{\mathrm{mig},V_O^{\cdot\cdot}}$ with the ability to accommodate a high concentration of randomly distributed oxygen vacancies and high thermodynamically stability, in order to produce a truly exceptional oxygen-ion conductor, remains to be seen.

Acknowledgments

Critical comments on the manuscript from Manfred Martin, Rainer Waser, Henning Schraknepper, Stefan Beschnitt, Annalena Schriever, and Amr Ramadan are gratefully acknowledged. Funding from the German Science Foundation (DFG) within the framework of the Collaborative Research Centre 'Nanoswitches' (SFB 917) is gratefully acknowledged.

Received: March 2, 2015
Revised: June 1, 2015
Published online: August 6, 2015

[1] P. Shewmon, *Diffusion in Solids*, TMS, Pennsylvania **1989**.
[2] H. Mehrer, *Diffusion in Solids*, Springer, Berlin, Heidelberg, New York **2007**.
[3] H. Schmalzried, *Festkoerperreaktion*, Verlag Chemie, Weinheim **1971**.
[4] R. W. Balluffi, S. M. Allen, W. C. Carter, *Kinetics of Materials*, John Wiley & Sons, New Jersey **2005**.
[5] R. J. Borg, G. J. Dienes, *An Introduction to Solid State Diffusion*, Academic Press, San Diego **1988**.
[6] J. Maier, *Physical Chemistry of Ionic Materials: Ions and Electrons in Solids*, J. Wiley & Sons, Chichester **2004**.
[7] R. E. Howard, A. B. Lidiard, *Rep. Prog. Phys.* **1964**, *27*, 161.
[8] C. Wagner, *Prog. Solid State Chem.* **1975**, *10*, Part 1, 3– 16.
[9] G. E. Murch in *Phase Transformations in Materials* (Ed: G. Kostorz), Wiley-VCH, Weinheim **2001**, pp. 173–238.
[10] A. Atkinson, *Solid State Ionics* **1984**, *12*, 309–320.
[11] M. Martin in *Diffusion in Condensed Matter* (Eds: P. Heitjans, J. Kaerger), Springer, Berlin Heidelberg New York, **2005**, pp 211–249.
[12] R. A. De Souza, M. Martin, *MRS Bull.* **2009**, *34*, 907–914.
[13] J. Janek, J. Sann, B. Mogwitz, M. Rohnke, M. Kleine-Boymann, *J. Korean Ceram. Soc.* **2012**, *49*, 56–65.
[14] T. Lee, H.-S. Kim, H.-I. Yoo, *Solid State Ionics* **2014**, *262*, 2–8.
[15] H. Hayashi, H. Inaba, M. Matsuyama, N. Lan, M. Dokiya, H. Tagawa, *Solid State Ionics* **1999**, *122*, 1–15.

[16] M. Mogensen, D. Lybye, N. Bonanos, P. Hendriksen, F. Poulsen, *Solid State Ionics* **2004**, *174*, 279–286.
[17] J. A. Kilner, A. Berenov, J. Rossiny in *Perovskite Oxide for Solid Oxide Fuel Cells* (Ed: T. Ishihara), Springer, Dordrecht Heidelberg London New York **2009**, pp 95–116.
[18] P. J. Harrop, *J. Mater. Sci.* **1968**, *3*, 206–222.
[19] R. Freer, *J. Mater. Sci.* **1980**, *15*, 803–824.
[20] G. Borchardt, K. Gömann, M. Kilo, H. Schmidt in *Ceramics Science and Technology*, Vol. *1* (Eds: R. Riedel, I. Chen), Wiley-VCH, Weinheim **2008**, Chapter 4, pp 105–180.
[21] G. H. Vineyard, *J. Phys. Chem. Solids* **1957**, *3*, 121–127.
[22] S. R. de Groot, P. Mazur, *Non-Equilibrium Thermodynamics*, North Holland, Amsterdam **1962**.
[23] D.-K. Lee, H.-I. Yoo, *Phys. Rev. Lett.* **2006**, *97*, 255901.
[24] C. Wagner, *Prog. Solid State Chem.* **1972**, *7*, 1–37.
[25] H.-S. Kim, H.-I. Yoo, *Phys. Chem. Chem. Phys.* **2011**, *13*, 4651–4658.
[26] I. Denk, F. Noll, J. Maier, *J. Am. Ceram. Soc.* **1997**, *80*, 279–285.
[27] J. Claus, M. Leonhardt, J. Maier, *J. Phys. Chem. Solids* **2000**, *61*, 1199–1207.
[28] T. Ishigaki, S. Yamauchi, K. Kishio, J. Mizusaki, K. Fueki, *J. Solid State Chem.* **1988**, *73*, 179–187.
[29] I. Kaur, Y. Mishin, W. Gust, *Fundamentals of Grain and Interphase Boundary Diffusion*, J. Wiley & Sons, Chichester **1995**.
[30] N. Peterson, *Int. Mater. Rev.* **1983**, *28*, 65–91.
[31] R. Balluffi, R. Mehl, *Metall. Trans. A* **1982**, *13*, 2069–2095.
[32] V. Metlenko, A. Ramadan, F. Gunkel, H. Du, H. Schraknepper, S. Hoffmann-Eifert, R. Dittmann, R. Waser, R. A. De Souza, *Nanoscale* **2014**, *6*, 12864–12876.
[33] R. A. De Souza, *Phys. Chem. Chem. Phys.* **2009**, *11*, 9939–9969.
[34] J.-H. Lee, *Monatsh. Chem.* **2009**, *140*, 1081–1094.
[35] R. A. De Souza, *Phys. Chem. Chem. Phys.* **2006**, *8*, 890–897.
[36] U. Balachandran, N. Eror, *J. Solid State Chem.* **1981**, *39*, 351–359.
[37] N. H. Chan, R. K. Sharma, D. M. Smyth, *J. Electrochem. Soc.* **1981**, *128*, 1762–1769.
[38] G. M. Choi, H. L. Tuller, D. Goldschmidt, *Phys. Rev. B* **1986**, *34*, 6972–6979.
[39] G. M. Choi, H. L. Tuller, *J. Am. Ceram. Soc.* **1988**, *71*, 201–205.
[40] R. Waser, T. Bieger, J. Maier, *Solid State Commun.* **1990**, *76*, 1077–1081.
[41] T. Bieger, J. Maier, R. Waser, *Solid State Ionics* **1992**, *5356*, Part 1, 578–582.
[42] R. Waser, *Z. Naturforsch.* **1987**, *42a*, 1357–1365.
[43] K. Kreuer, *Solid State Ionics* **1999**, *125*, 285–302.
[44] N. Sata, K. Hiramoto, M. Ishigame, S. Hosoya, N. Niimura, S. Shin, *Phys. Rev. B* **1996**, *54*, 15795–15799.
[45] R. Waser, *J. Am. Ceram. Soc.* **1991**, *74*, 1934–1940.
[46] I. Denk, W. Münch, J. Maier, *J. Am. Ceram. Soc.* **1995**, *78*, 3265–3272.
[47] R. Moos, K. H. Härdtl, *J. Am. Ceram. Soc.* **1997**, *80*, 2549–2562.
[48] C.-J. Shin, H.-I. Yoo, C.-E. Lee, *Solid State Ionics* **2007**, *178*, 1081–1087.
[49] C.-J. Shin, H.-I. Yoo, *Solid State Ionics* **2007**, *178*, 1089–1094.
[50] K. Gömann, G. Borchardt, A. Gunhold, W. Maus-Friedrichs, H. Baumann, *Phys. Chem. Chem. Phys.* **2004**, *6*, 3639–3644.
[51] K. Gömann, G. Borchardt, M. Schulz, A. Gömann, W. Maus-Friedrichs, B. Lesage, O. Kaitasov, S. Hoffmann-Eifert, T. Schneller, *Phys. Chem. Chem. Phys.* **2005**, *7*, 2053–2060.
[52] M. J. Akhtar, Z.-U.-N. Akhtar, R. A. Jackson, C. R. A. Catlow, *J. Am. Ceram. Soc.* **1995**, *78*, 421–428.
[53] J. Crawford, P. Jacobs, *J. Solid State Chem.* **1999**, *144*, 423–429.
[54] B. Thomas, N. Marks, B. Begg, *Nucl. Instrum. Methods Phys. Res. Sect. B* **2007**, *254*, 211–218.
[55] A. Walsh, C. R. A. Catlow, A. G. H. Smith, A. A. Sokol, S. M. Woodley, *Phys. Rev. B* **2011**, *83*, 220301.
[56] T. Mizoguchi, N. Takahashi, H.-S. Lee, *Appl. Phys. Lett.* **2011**, *98*, 091909.
[57] A. H. H. Ramadan, N. L. Allan, R. A. De Souza, *J. Am. Ceram. Soc.* **2013**, *96*, 2316–2321.
[58] R. A. De Souza, V. Metlenko, D. Park, T. E. Weirich, *Phys. Rev. B* **2012**, *85*, 174109.
[59] R. A. De Souza, F. Gunkel, S. Hoffmann-Eifert, R. Dittmann, *Phys. Rev. B* **2014**, *89*, 241401.
[60] N.-H. Chan, R. Sharma, D. Smyth, *J. Am. Ceram. Soc.* **1981**, *64*, 556–562.
[61] H.-I. Yoo, C.-R. Song, D.-K. Lee, *J. Electroceram.* **2002**, *8*, 5–36.
[62] D. M. Smyth, *J. Electroceram.* **2003**, *11*, 89–100.
[63] S. Lee, C. A. Randall, *Solid State Ionics* **2013**, *249250*, 86–92.
[64] U. Balachandran, B. Odekirk, N. Eror, *J. Solid State Chem.* **1982**, *41*, 185–194.
[65] U. Balachandran, B. Odekirk, N. Eror, *J. Mater. Sci.* **1982**, *17*, 1656–1662.
[66] M. Zhou, T. Bak, J. Nowotny, M. Rekas, C. Sorrell, E. Vance, *J. Mater. Sci.: Mater. Electron.* **2002**, *13*, 697–704.
[67] K. A. Müller, *J. Phys. France* **1981**, *42*, 551–557.
[68] R. Merkle, J. Maier, *Phys. Chem. Chem. Phys.* **2003**, *5*, 2297–2303.
[69] M. Schie, R. Waser, R. A. De Souza, *J. Phys. Chem. C* **2014**, *118*, 15185–15192.
[70] J. Haeng Yu, J.-S. Lee, J. Maier, *Phys. Chem. Chem. Phys.* **2005**, *7*, 3560–3564.
[71] M. Cherry, M. S. Islam, J. D. Gale, C. R. A. Catlow, *J. Phys. Chem.* **1995**, *99*, 14614–14618.
[72] R. Meyer, R. Waser, J. Helmbold, G. Borchardt, *Phys. Rev. Lett.* **2003**, *90*, 105901.
[73] K. Sasaki, J. Claus, J. Maier, *Solid State Ionics* **1999**, *121*, 51–60.
[74] H.-I. Yoo, T.-S. Oh, H.-S. Kwon, D.-K. Shin, J.-S. Lee, *Phys. Chem. Chem. Phys.* **2009**, *11*, 3115–3126.
[75] R. A. De Souza, M. Martin, *Phys. Chem. Chem. Phys.* **2008**, *10*, 2356–2367.
[76] L. G. Harrison, *Trans. Faraday Soc.* **1961**, *57*, 1191–1199.
[77] H. Schraknepper, R. A. De Souza, unpublished.
[78] R. Waser, R. Hagenbeck, *Acta Mater.* **2000**, *48*, 797–825.
[79] R.-V. Wang, P. C. McIntyre, *J. Appl. Phys.* **2005**, *97*, 023508.
[80] S. Gottschalk, H. Hahn, S. Flege, A. G. Balogh, *J. Appl. Phys.* **2008**, *104*, 114106.
[81] M. F. Kessel, R. A. De Souza, M. Martin, *Phys. Chem. Chem. Phys.* **2015**, *17*, 12587–12597.
[82] C. Schwab, H. Schraknepper, R. A. De Souza, unpublished.
[83] I. Sakaguchi, H. Haneda, *J. Solid State Chem.* **1996**, *124*, 195–197.
[84] X. Guo, *Science* **2009**, *324*, 465.
[85] A. Cavallaro, M. Burriel, J. Roqueta, A. Apostolidis, A. Bernardi, A. Tarancón, R. Srinivasan, S. N. Cook, H. L. Fraser, J. A. Kilner, D. W. McComb, J. Santiso, *Solid State Ionics* **2010**, *181*, 592–601.
[86] C. C. Wang, C. M. Lei, G. J. Wang, X. H. Sun, T. Li, S. G. Huang, H. Wang, Y. D. Li, *J. Appl. Phys.* **2013**, *113*, 094103.
[87] D. B. Schwarz, H. U. Anderson, *J. Electrochem. Soc.* **1975**, *122*, 707–710.
[88] P. Pasierb, S. Komornicki, M. Rekas, *J. Phys. Chem. Solids* **1999**, *60*, 1835–1844.
[89] M. Leonhardt, R. A. De Souza, J. Claus, J. Maier, *J. Electrochem. Soc.* **2002**, *149*, J19–J26.
[90] K. Kerman, C. Ko, S. Ramanathan, *Phys. Chem. Chem. Phys.* **2012**, *14*, 11953–11960.
[91] A. E. Paladino, L. G. Rubin, J. S. Waugh, *J. Chem. Phys. Solids* **1965**, *26*, 391–397.
[92] F. D. Gealy, H. L. Tuller, *J. Phys. Colloques* **1990**, *51*, 483–487.
[93] J. Blanc, D. L. Staebler, *Phys. Rev. B* **1971**, *4*, 3548–3557.

[94] A. Hackmann, O. Kanert, *Radiat. Eff. Defects Solids* **1991**, *119–121*, 651–656.
[95] F. Cordero, *Phys. Rev. B* **2007**, *76*, 172106.
[96] D. D. Cuong, B. Lee, K. M. Choi, H.-S. Ahn, S. Han, J. Lee, *Phys. Rev. Lett.* **2007**, *98*, 115503.
[97] M. Lontsi-Fomena, A. Villesuzanne, J.-P. Doumerc, C. Frayret, M. Pouchard, *Comput. Mater. Sci.* **2008**, *44*, 53–60.
[98] R. A. De Souza, A. H. H. Ramadan, *Phys. Chem. Chem. Phys.* **2013**, *15*, 4505–4509.
[99] C. Schaffrin, *Phys. Status Solidi A* **1976**, *35*, 79–88.
[100] K. Watanabe, I. Sakaguchi, S. Hishita, H. Haneda, N. Ohashi, *Key Eng. Mater.* **2013**, *566*, 262–265.
[101] M. Leonhardt, J. Jamnik, J. Maier, *Electrochem. Solid-State Lett.* **1999**, *2*, 333–335.
[102] J. S. Waugh, A. E. Paladino, B. DiBenedetto, R. Wantman, *J. Am. Ceram. Soc.* **1963**, *46*, 60–60.
[103] J. C. Amante, J. D. Crawley, J. Kim, T. R. Lemberger in *Point Defects and Related Properties of Ceramics, Ceramic Trans* (Eds: T. Mason, J. L. Routbort), American Ceramics Society, Westerville, OH, USA, **1991**, pp 303–312.
[104] K. Szot, W. Speier, R. Carius, U. Zastrow, W. Beyer, *Phys. Rev. Lett.* **2002**, *88*, 075508.
[105] D. Marrocchelli, L. Sun, B. Yildiz, *J. Am. Chem. Soc.* **2015**, *137*, 4735–4748.
[106] P. C. McIntyre, *J. Am. Ceram. Soc.* **2000**, *83*, 1129–1136.
[107] S. P. Waldow, R. A. De Souza, unpublished.
[108] R. A. De Souza, M. J. Pietrowski, U. Anselmi-Tamburini, S. Kim, Z. A. Munir, M. Martin, *Phys. Chem. Chem. Phys.* **2008**, *10*, 2067–2072.
[109] C. Fisher, H. Matsubara, *Solid State Ionics* **1998**, *113–115*, 311–318.
[110] W. George, R. Grace, *J. Phys. Chem. Solids* **1969**, *30*, 889–892.
[111] B. Gautason, K. Muehlenbachs, *Science* **1993**, *260*, 518–521.
[112] T. Bak, J. Nowotny, C. Sorrel, *J. Phys. Chem. Solids* **2004**, *65*, 1229–1241.
[113] M. Raymond, D. Smyth, *J. Phys. Chem. Solids* **1996**, *57*, 1507–1511.
[114] B. J. Kennedy, C. J. Howard, B. C. Chakoumakos, *J. Phys. Condens. Matter* **1999**, *11*, 1479.
[115] B. Noheda, D. E. Cox, G. Shirane, R. Guo, B. Jones, L. E. Cross, *Phys. Rev. B* **2000**, *63*, 014103.
[116] V. V. Prisedsky, V. I. Shishkovsky, V. V. Klimov, *Ferroelectrics* **1977**, *17*, 465–468.
[117] H. G. Bohn, T. Schober, *J. Am. Ceram. Soc.* **2000**, *83*, 768–772.
[118] S. Tao, J. T. Irvine, *J. Solid State Chem.* **2007**, *180*, 3493–3503.
[119] I. Ahmed, S.-G. Eriksson, E. Ahlberg, C. Knee, H. Götlind, L.-G. Johansson, M. Karlsson, A. Matic, L. Börjesson, *Solid State Ionics* **2007**, *178*, 515–520.
[120] J. Labrincha, F. Marques, J. Frade, *J. Mater. Sci.* **1995**, *30*, 2785–2792.
[121] J. Müller, K. Kreuer, J. Maier, S. Matsuo, M. Ishigame, *Solid State Ionics* **1997**, *97*, 421–427.
[122] T. Schober, *Solid State Ionics* **2001**, *145*, 319–324.
[123] N. Kurita, N. Fukatsu, K. Ito, T. Ohashi, *J. Electrochem. Soc.* **1995**, *142*, 1552–1559.
[124] R. A. De Souza, J. A. Kilner, C. Jeynes, *Solid State Ionics* **1997**, *97*, 409–419.
[125] K. Kobayashi, S. Yamaguchi, Y. Iguchi, *Solid State Ionics* **1998**, *108*, 355–362.
[126] M. P. Hills, C. Schwandt, R. V. Kumar, *J. Electrochem. Soc.* **2006**, *153*, H189–H194.
[127] J. Bao, Y. Okuyama, Z. Shi, N. Fukatsu, N. Kurita, *Mater. Trans.* **2012**, *53*, 973–979.
[128] H. Iwahara, T. Yajima, T. Hibino, K. Ozaki, H. Suzuki, *Solid State Ionics* **1993**, *61*, 65–69.
[129] T. Norby in *Perovskite Oxide for Solid Oxide Fuel Cells* (Ed: T. Ishihara), Springer, Dordrecht Heidelberg London New York **2009**, pp 217–241.
[130] Y. Yamazaki, P. Babilo, S. M. Haile, *Chem. Mater.* **2008**, *20*, 6352–6357.
[131] E. Fabbri, D. Pergolesi, E. Traversa, *Chem. Soc. Rev.* **2010**, *39*, 4355–4369.
[132] T. Schober, H. Bohn, *Solid State Ionics* **2000**, *127*, 351–360.
[133] A. C. T. van Duin, B. V. Merinov, S. S. Han, C. O. Dorso, W. A. Goddard, *J. Phys. Chem. A* **2008**, *112*, 11414–11422.
[134] K. D. Kreuer, W. Münch, M. Ise, T. He, A. Fuchs, U. Traub, J. Maier, *Ber. Bunsenges. Phys. Chem.* **1997**, *101*, 1344–1350.
[135] M. Oishi, S. Akoshima, K. Yashiro, K. Sato, J. Mizusaki, T. Kawada, *Solid State Ionics* **2008**, *179*, 2240–2247.
[136] T. He, K. Kreuer, Y. Baikov, J. Maier, *Solid State Ionics* **1997**, *95*, 301–308.
[137] E. Bertolo, J. Kilner, M. Sahibzada, *J. Solid State Electrochem.* **2004**, *8*, 585–591.
[138] T. Ishihara, J. A. Kilner, M. Honda, N. Sakai, H. Yokokawa, Y. Takita, *Solid State Ionics* **1998**, *113115*, 593–600.
[139] L. Wang, R. Merkle, J. Maier, T. Acartrk, U. Starke, *Appl. Phys. Lett.* **2009**, *94*, 071908.
[140] M. Li, M. J. Pietrowski, R. A. De Souza, H. Zhang, I. M. Reaney, S. N. Cook, J. A. Kilner, D. C. Sinclair, *Nat. Mater.* **2014**, *13*, 31–35.
[141] G. Zhang, D. Smyth, *Solid State Ionics* **1995**, *82*, 161–172.